THE ASTROPHYSICAL JOURNAL, 344:376–398, 1989 September 1

A SPECTROSCOPIC, PHOTOMETRIC, AND X-RAY STUDY OF THE DQ HERCULIS SYSTEM 1H0542−407

D. A. H. BUCKLEY AND I. R. TUOHY
Mount Stromlo and Siding Spring Observatories, Australian National University
Received 1988 July 25; accepted 1989 January 26

ABSTRACT

We report spectroscopic and photometric observations of the DQ Herculis binary 1H0542−407 and derive models based upon these and our earlier X-ray observations.

Time-resolved spectroscopy has revealed radial velocity variations at two periods: the 5.7 hr orbital and 31.9 minute white dwarf rotation periods. These periods are consistent with those previously derived by us from our X-ray observations with *EXOSAT*. The orbital semiamplitude velocity is low, ~ 50 km s^{-1}, leading to a mass function of $3.3 \pm 0.6 \times 10^{-3}\ M_\odot$ and an orbital inclination $<25°$. We attribute the spin-modulated, low-amplitude, velocity variation ($K \sim 20$ km s^{-1}) to a shocked region, corotating with the white dwarf at the magnetosphere/accretion disk boundary. It is in this region where most of the He II and narrower Balmer emission is produced. The broad Balmer line component is interpreted as arising from a truncated accretion disk, which we model as a standard Shakura-Sunyaev α-disk.

Extensive high speed and *UBVRI* photometry of 1H0542−407 has also been obtained. A time series analysis has identified several periods, including the orbital sidebands $\nu - 2\omega$, $\nu - \omega$, and $\nu + \omega$ (where ν, ω are the spin and orbital frequencies). The dominant optical period occurs at $\nu - \omega$, i.e., a period of 35.1 minutes, which we attribute to X-rays reprocessed in a region fixed in the orbital frame of reference (i.e., the disk hot-spot/bulge and/or the secondary star).

The optical and X-ray periods, and the pulse fractions, are explained in terms of accretion in an auroral arc near the magnetic poles. The resulting thermal bremsstrahlung X-rays are modulated at the spin period due to significant opacity variation as a function of viewing angle. This results in a fan beam which sweeps over the accretion/disk and secondary star as the white dwarf rotates. The consequent reprocessing of X-rays in the hot spot and secondary star produces the sideband optical period. We invoke X-ray reflection of the harder (>2 keV) X-rays to explain the presence of the sideband period in the X-ray data.

Our model for this system consists of a 1.3 $M_\odot$ white dwarf and a 0.57 $M_\odot$ M0 V secondary with an orbital period of 5.7 hr and an inclination $\sim 25°$. An accretion disk extends from roughly seven white dwarf radii out to 90% of the mean Roche lobe radius. The inferred magnetic field strength is in the region 1–10 MG, while the X-ray luminosity is ~ 5–10×10^{34} ergs s^{-1}. Several independent methods point to a distance of $\gtrsim 500$ pc.

Subject headings: stars: binaries — stars: dwarf novae — stars: individual (1H0542−407) — stars: magnetic — X-rays: binaries

I. INTRODUCTION

As a class, the DQ Herculis magnetic variables, which now number ~ 15, exhibit properties somewhat intermediate between the synchronously rotating, diskless, AM Herculis systems (or polars), and the vast majority of "normal," or nonmagnetic ($B \leq 10^5$ G), cataclysmic variables (hereafter CVs). The defining characteristic of a DQ Her variable is the asynchronous rotation of the white dwarf primary, which is manifested in the X-ray–emitting subclass of DQ Her binaries, the intermediate polars (which are the majority), as X-ray and usually optical pulsations at the rotation period (see reviews, e.g., Warner 1983, 1985; Mason 1985; Berriman 1988).

Taken as a group, the DQ Her stars (or intermediate polars) have an orbital period distribution statistically identical to the more numerous nonmagnetic CVs (Schmidt and Liebert 1987). The AM Her star are shorter period systems, mostly populating the region below the 2–3 hr period gap (King, Frank, and Ritter 1985).

It is appealing to believe that there is an evolutionary sequence between the longer period, asynchronously rotating DQ Her systems, and the shorter period, synchronous AM Her systems (Chanmugam and Ray 1984; King 1985; King, Frank, and Ritter 1985; Hameury, King, and Lasota 1986; Hameury *et al.* 1987). If such an evolutionary senario is indeed correct, and hence the magnetic moments of the two classes are similar, then we expect to see evidence of strong ($\gtrsim 20$ MG) surface magnetic fields. Opponents of the above theory point to the lack of observational evidence, for example, the low polarizations (e.g., Cropper 1986) and absence of Zeeman effects in DQ Her systems. The debate continues as to what the field strengths are in DQ Her systems and if they are in some way connected to the AM Her binaries. The optical to X-ray nature of systems with strong fields has been discussed by King (1985), Lamb (1983, 1985), and Imamura and Durisen (1983). Central to the argument over field strengths in DQ Her binaries is the presence or absence of accretion disks, possibly in a truncated form. King, Frank, and Ritter (1985) argue that disks will only be present in systems with periods greater than ~ 5 hr. However, Lamb and Melia (1987) show that while disk *formation* may be prevented under certain circumstances, disks already *existing* will remain intact, at least partially, under

those same conditions. They identified several regimes, parameterized by the magnetic moment μ, for which systems exhibited characteristics ranging from AM Her (high μ), DQ Her (intermediate μ) to nonmagnetic CVs (low μ). The current observational evidence seems to favor the presence of accretion disks in DQ Her systems, even in some short-period systems (e.g., EX Hya; Hellier *et al.* 1987), which implies that the AM Her and DQ Her binaries do not have the same μ values.

In this paper we present new observations of 1H0542−407, a DQ Her system discovered by us (Tuohy *et al.* 1986; hereafter Paper I) through our *HEAO 1* X-ray source identification program (e.g., Buckley, Tuohy, and Remillard 1985). In Paper I, we presented analysis of *EXOSAT* observations and *UBVRI* photometry which conclusively showed 1H0542−407 to be a DQ Her system, or intermediate polar. We derived a white dwarf spin period of 1920 ± 20 s and an orbital period of 6.2 ± 0.5 hr. In the current paper we present and interpret results of time series analyses on spectroscopic and photometric data. A preliminary presentation of some of these data has appeared in an earlier paper (Buckley and Tuohy 1987). In the present paper we expand on and develop models based upon the theoretical accretion conditions expected for this system which adequately account for the spectroscopic, photometric, and X-ray observations. We compare our results to other DQ Her systems and address some outstanding problems in the interpretation of common observational properties.

II. SPECTROSCOPY

a) Observations

Spectra were taken of 1H0542−407 using the 3.9 m Anglo-Australian Telescope (AAT) on the nights of 1985 November 17 and 18. Simultaneous coverage was achieved in the two spectral regions 3930–4960 Å and 5300–11000 Å, hereafter referred to as the "blue" and "red" spectra, respectively. The blue spectra were taken with the RGO spectrograph at a reciprocal dispersion of $\sim$0.5 Å pixel^{-1} and a resolution of $\sim$1.3 Å. The detector was the Image Photon Counting System (IPCS). A dichroic was used to divert the red wavelengths ($\geq$5300 Å) to the Faint Object Red Spectrograph (FORS), which employs a GEC CCD (584 pixels). Most of the first night was badly affected by cloud, with only $\sim$3 hr of useful data collected. Conditions were clear on the second night, and $\sim$6 hr of continuous data were collected on 1H0542−407.

The high-speed mode of operation for the IPCS (Bailey 1984; Watts *et al.* 1986) was employed on both nights. Individually recorded IPCS frames were summed during the data reduction phase over $\sim$100 s for the stronger emission lines Hβ, Hγ, Hδ, and He II λ4686. For the weaker lines, He I λ4026, λ4387, λ4471, λ4920, C III–N III $\lambda\lambda$4640–4650 and Hϵ, the minimum time resolution was $\sim$300 s. We produced two sets of spectroscopic data corresponding to these two exposure times, hereafter referred to as the "100 s data" and the "300 s data." For the 100 s data we obtained a total of 79 and 153 spectra on the two respective nights, while for the 300 s data there were 21 and 47 spectra.

We did not observe any flux standards (due to an incorrect pointing), and hence our spectra are unfluxed. Seeing on both nights was $\leq 2''$. The spectrograph slit was rotated to exclude most of the light from the star adjacent ($\sim 4''$) to 1H0542−407 (see Paper I).

In Figures 1*a* and 1*b* we show representative blue and red spectra of 1H0542−407. The data consist of a grand sum, with no corrections for velocity variations. The blue spectrum is essentially identical to the discovery spectrum presented in Paper I. The red spectrum shows the prominent Paschen series, He I lines and possibly O I λ7777. There is no evidence of significant absorption features which might be attributable to a late-type secondary star, although we emphasize that these data are of low resolution ($\sim$20 Å).

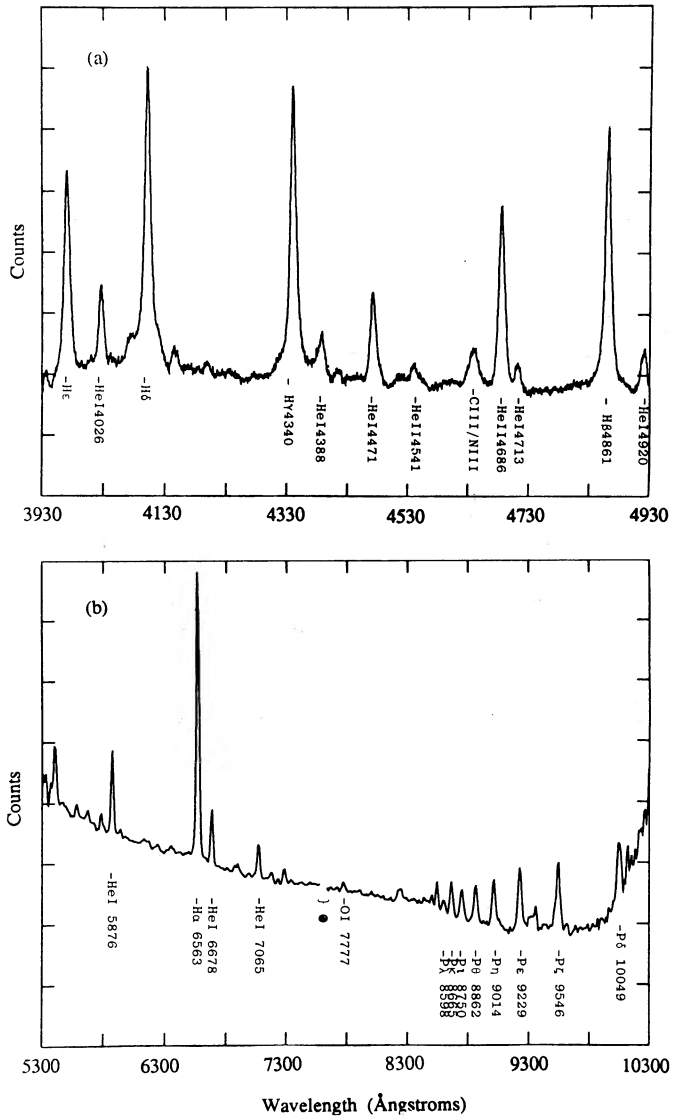

FIG. 1.—(*a*) Blue AAT grand sum spectrum of 1H0542−407 taken using the IPCS on 1985 November 17 and 18 (unfluxed). (*b*) Red AAT grand sum spectrum of 1H0542−407 taken using FORS on 1985 November 17 and 18 (unfluxed). The rise in counts beyond about $P\delta$ is an artifact due to the overlapping second order.

b) Radial Velocity Measurements

On inspection of the blue spectra we found that for the 100 s data, all the emission lines seemed to be well represented by a single Gaussian profile of FWHM $\sim$1200 km s^{-1}. For the higher signal to noise 300 s data, a second broad (FWHM $\sim$2500 km s^{-1}) Gaussian component was required to fit the wings of the Balmer lines. We then adopted a Gaussian profile least-squares fitting algorithm to determine the line profile parameters for both sets of data. In Figures 2 and 3 we show a

representative sample of the variations of the velocity, sigma, and equivalent width for the Hβ and He II λ4686 lines. The amplitude of the emission lines was found to vary in the same manner as the total intensity summed over the continuum, and hence this variation is not intrinsic to the line. Immediately obvious is the sinusoidal radial velocity variation with a period of 5–6 hr and a velocity semiamplitude of $K \sim 50$–60 km s^{-1}. Also apparent in these data are short time scale ($\sim$2000 s) velocity excursions, which are seen most clearly in the November 17 data. This behavior is reminiscent of that seen by Penning (1985) in four long-period DQ Her systems, V1223 Sgr, FO Aqr, BG CMi, and AO Psc, which he associated with the white dwarf rotation period. In the case of 1H0542−407 the short-period variation is similar, but at a lower amplitude than the other systems. In a later section (§ IIc) we show that the period is indeed the spin period of the white dwarf.

The radial velocities of the broad Balmer components showed considerable scatter with no clear trend, probably as a result of the ill conditioning of the least-squares method applied to a very broad feature which has a small velocity amplitude (very much smaller than its velocity width).

Radial velocity variations were also derived for the Balmer lines using a cross-correlation technique on the entire spectrum, except for non-Balmer lines (He I, He II, C III–N III) which were excised from the data and replaced by a local average of the continuum. The result of this method was to improve the errors considerably and confirm the short-period radial velocity variation. In Figure 4*a* we show the radial velocity curve derived using this method.

c) *Radial Velocity Curves*

Since both the 100 s and 300 s data sets showed clear evidence of two periods, we fitted double sine curves to the combined nights' data using a χ^2 minimization routine. The results of these fits are shown for the He II λ4686 line in Figures 4*b* and 4*c* for both nights. In Table 1 we present the radial velocity curve parameters for the stronger lines. The weaker lines show similar behavior. Initially we determined the parameters separately for each night; however, the long-period sinusoid is poorly constrained on the first night. Fitting both nights simultaneously gave a much better determination of the long period. We have determined this longer period to be 5.7 hr from all our velocity curve solutions and identify it as the orbital period of 1H0542−407. The value is within the limits set by us in Paper I based on our X-ray light curves, namely 6.2 $\pm$ 0.5 hr. We find that the best value for the short period as determined from our radial velocity analysis is 1908 $\pm$ 10 s, in excellent agreement with the dominant X-ray period in the *EXOSAT* LE1 light curve of 1920 $\pm$ 20 s (Paper I). One-day aliases were a problem for the short period; however, the adopted period has the

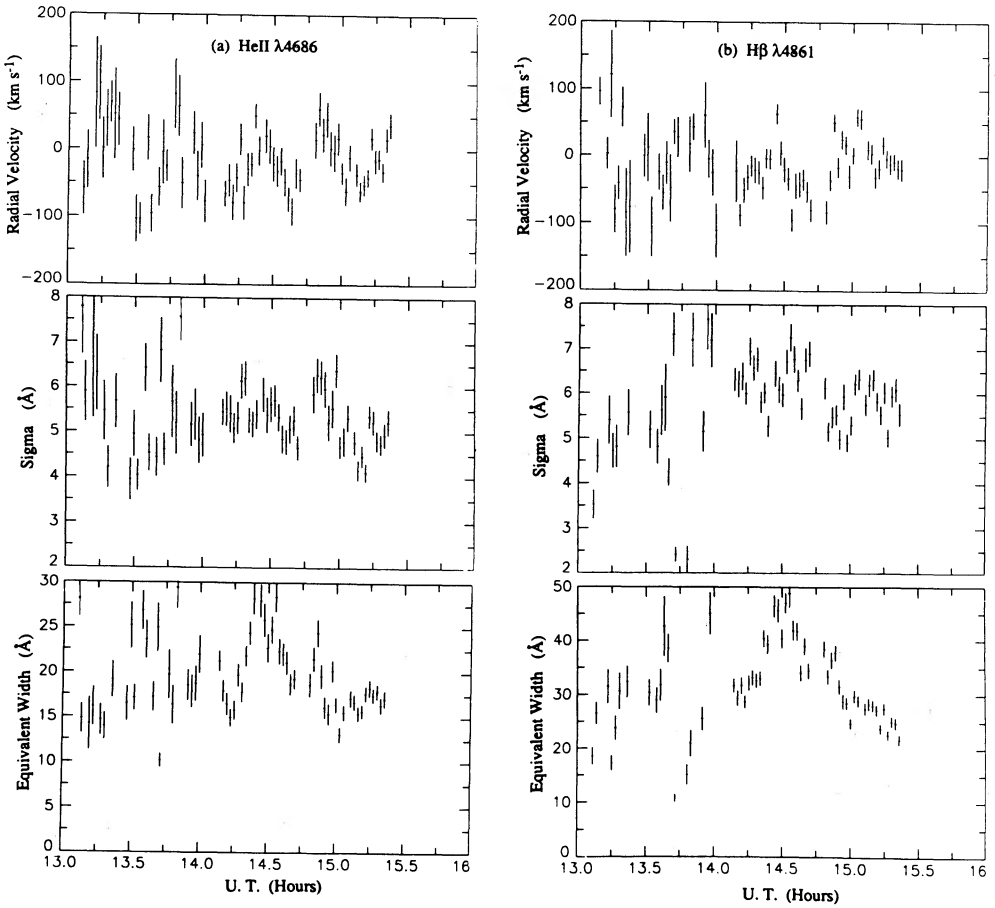

FIG. 2.—(*a*) Emission-line parameter variations (velocity, sigma, and equivalent width) for the line He II λ 4686 on 1985 November 17. (*b*) Emission-line parameter variations (velocity, sigma, and equivalent width) for the line Hβ on 1985 November 17.

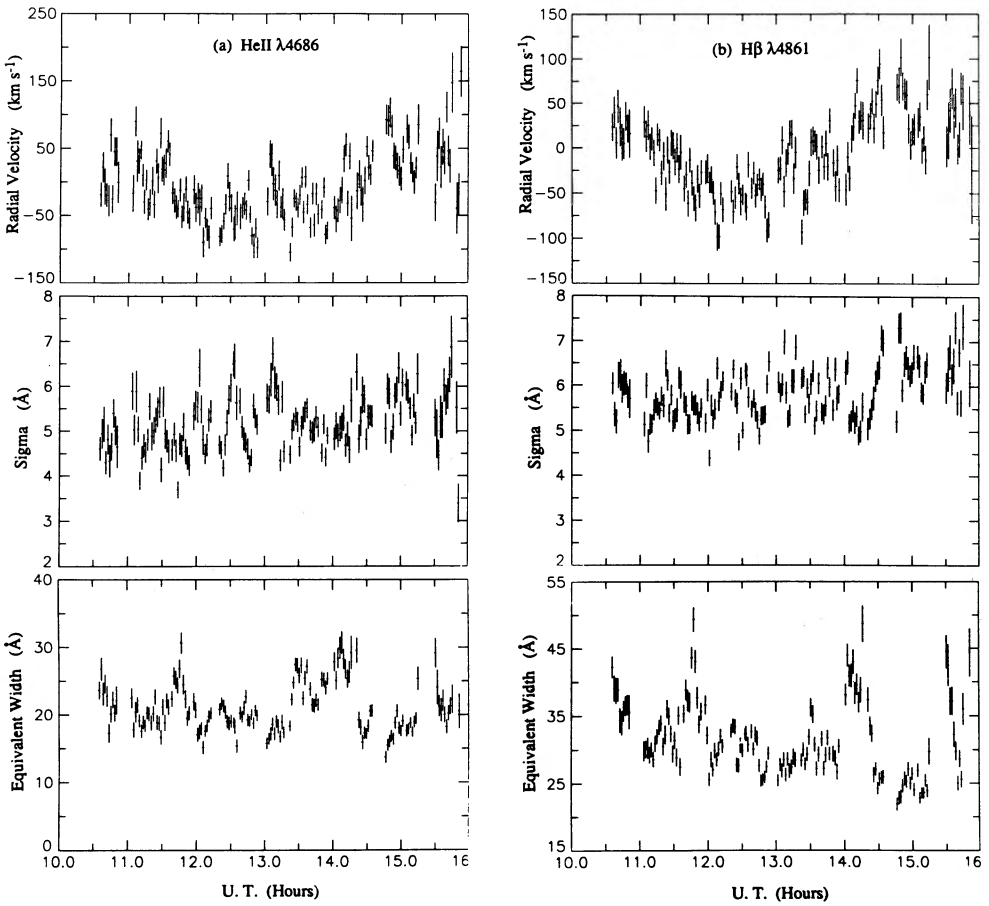

FIG. 3.—(*a*) Emission-line parameter variations (velocity, sigma, and equivalent width) for the line He II λ 4686 on 1985 November 18. (*b*) Emission-line parameter variations (velocity, sigma, and equivalent width) for the line Hβ on 1985 November 18.

lowest χ^2 value and corresponds to the best agreement between solutions for different lines.

We utilized two period-finding techniques to confirm the short-period sine fit results. One of the methods was based upon epoch folding, as described in Paper I, while the other was a discrete Fourier transform (hereafter DFT) technique for unequally spaced data, similar to that of Deeming (1975). The search interval was confined between 1000 s and 3000 s. Despite the one-day aliases, both methods confirmed the ~1910 s periodicity.

d) Binned Spectra

The periods found in § II*c* were used to rebin all of the spectra into orbital and rotational phase bins. We chose 5, 10, and 15 phase bins per period, and the resultant spectra were then reanalyzed. The major aim of this exercise was to investigate in detail the line profile variations at the orbital and rotational periods. Of particular interest was the broad component of the Balmer lines, where we aimed at a more accurate determination of their velocity variations. We therefore repeated our Gaussian fitting technique on the rebinned data, and in Figure 5 we show the most important outcome of this exercise, namely the He II λ4686 velocity, sigma, and equivalent width variation over the rotation cycle.

e) The Broad Component

In order to investigate the broad component of the Balmer lines, we developed a line-measuring technique sensitive to the wings of the emission lines. The algorithm we used was similar to the Gaussian convolution scheme of Schneider and Young

TABLE 1

RADIAL VELOCITY CURVE PARAMETERS

Parameter	He II λ4686	Hβ	Hγ	Hδ	He I λ4471
γ (km s^{-1})	1 ± 4	3 ± 2	23 ± 3	4 ± 3	45 ± 5
K_1 (km s^{-1})	53 ± 4	51 ± 3	55 ± 4	52 ± 4	58 ± 7
P_1 (hr)	5.71 ± .04	5.66 ± .03	5.68 ± .03	5.77 ± .02	5.77 ± .07
K_2 (km s^{-1})	23 ± 4	18 ± 3	20 ± 3	23 ± 3	24 ± 6
P_2 (hr)[a]	0.530	0.531	0.530	0.532	0.530

[a] All ±0.003 hr.

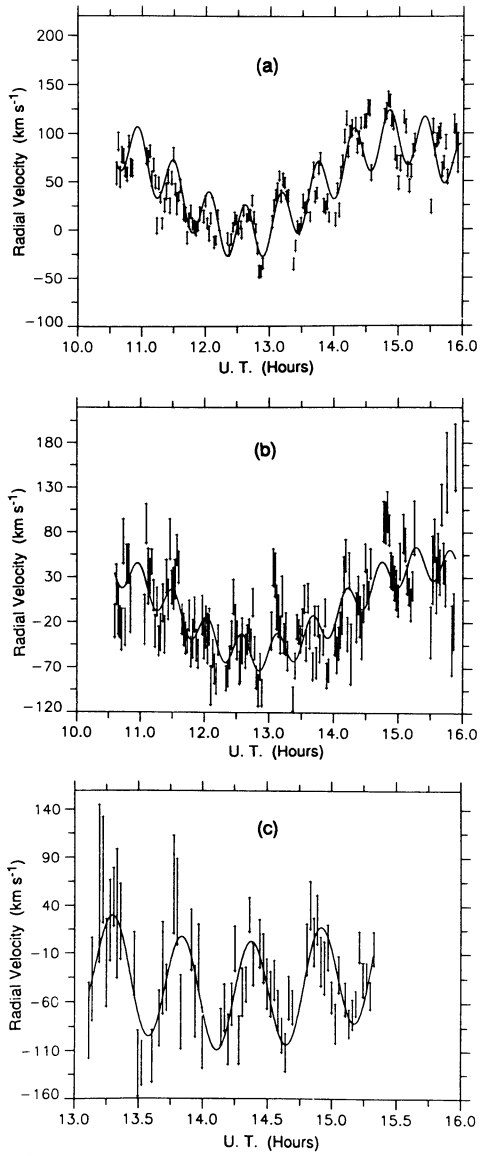

FIG. 4.—(*a*) Balmer cross-correlation velocities plus two-sine radial velocity curve solution for the 100 s exposure spectra taken on 1985 November 18. (*b*) He II λ4686 velocities plus two-sine radial velocity curve solution for the 100 s exposure spectra taken on 1985 November 18. (*c*) He II λ4686 velocities plus two-sine radial velocity curve solution for the 100 s exposure spectra taken on 1985 November 17.

Time axis is hours of universal time on the date of the observation.

(1980), Shafter (1983, 1985), Shafter, Szkody, and Thorstensen (1986), Horne and Marsh (1986), and Hessman (1988). Basically the line profile is masked by two Gaussian passbands, one in the red and another in the blue, of fixed width and separation which move through the profile, from one side to the other, until the counts in the two passbands, or "filters," are equal. The midposition of the filters at this point then defines the line center.

We probed the wings in steps as far out as ~20 Å in the blue and red. Individual radial velocities were then derived for the lines Hβ, Hγ, and Hδ at each of these wing positions and a single sinusoidal curve was fitted to the data. Contrary to many other systems (e.g., Shafter 1983), 1H0542−407 shows no significant change in the radial velocity parameters (γ, *K*, *P*, φ). In Table 2 we list the parameters γ and *K* for various values of the separation of the red and blue wings, *a*, and Gaussian width, σ.

Our conclusion is that the velocities derived from the line wings are no different from those derived from the Gaussian fitting techniques, the former of which are produced in the inner disk regions and therefore more closely follow the white dwarf's orbital motion. Our models, to be presented in later sections, based on the derived semiamplitude velocities are therefore not seriously compromised by line profile complexities.

f) *Spectroscopic Evidence for a Bulge*

We rebinned all of our 100 s spectra for both nights into five orbital and rotational phase bins according to the periods given in § IIc. We again fitted a Gaussian to the dominant narrower component in the lines Hδ, Hγ, Hβ, and He II λ4686. This fit was then substracted from the data to give a residual spectrum. In the case of the three Balmer lines, the resulting profile is the broad component, which we will later attribute to the accretion disk (§ V*d*). Also present in the residual Balmer profiles is a sharp feature which is seen in all five rotational phase bins at an approximately constant velocity position, but

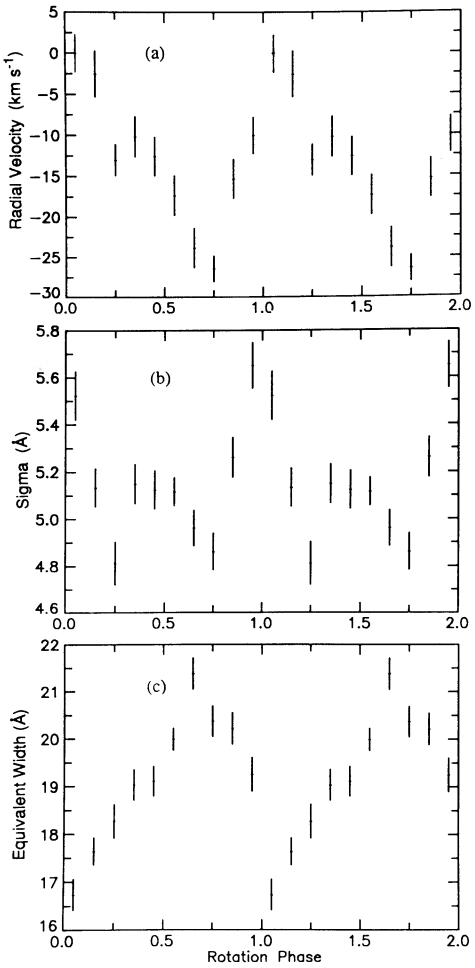

FIG. 5.—(*a*) Radial velocity, (*b*) sigma, and (*c*) equivalent width variations of the He II λ4686 line folded at the white dwarf rotation period of 1911 s. Two cycles are shown for clarity.

TABLE 2

RADIAL VELOCITY CURVE PARAMETERS DERIVED FROM GAUSSIAN FILTER METHOD

		He II		Hβ		Hγ		He I	
a (Å)	σ (Å)	γ (km s^{-1})	K (km s^{-1})	γ (km s^{-1})	K (km s^{-1})	γ (km s^{-1})	K (km s^{-1})	γ (km s^{-1})	K (km s^{-1})
5.....	5	30.3	47.4	15.2	51.0	34.1	49.3	63.8	52.7
10.....	5	30.1	46.9	13.3	51.7	34.4	50.2	69.8	53.3
15.....	5	29.8	45.8	9.6	52.9	34.9	51.6	80.5	54.5
20.....	5	29.5	43.9	3.7	54.8	35.6	54.0	96.4	55.8
30.....	5	49.6	45.7	−17.3	59.6	28.8	53.7	115.1	54.3

is only visible in three of the orbital phase bins. Furthermore, the velocity of this feature varies roughly in antiphase with the disk/white dwarf velocity as derived in § IIc. The situation is more compelling in the case of the He II line, where we clearly see that for at least two orbital phase bins, the profiles show opposite asymmetries. This can be seen in Figure 6 where we plot the He II line, plus the fitted dominant Gaussian, and the residual profile. An explanation of this behavior is the superposition of a narrower "core" component, moving in antiphase, with a broader component. We have determined the position of this core from measuring the centroid of the sharp feature in the residual spectrum. The velocities vary in the same sense as the Balmer lines, but with a greater amplitude, from roughly −160 to 160 km s^{-1}. Our conclusion is that we are observing the S-wave of the disk hot spot.

III. PHOTOMETRY

Photometry of 1H0542−407 was undertaken during four observing runs in 1984 November and 1985 January, November, and December. Two types of observations were conducted: *UBVRI* simultaneous photometry and high time resolution (200 ms) monitoring.

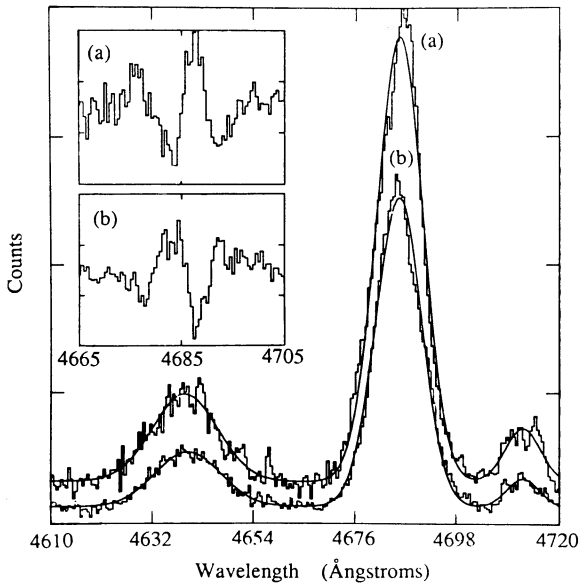

FIG. 6.—The rebinned He II λ4686 line at rotation phase (*a*) 0.2 and (*b*) 0.5 superposed with the single Gaussian component fit. *Insets* (*a*), (*b*): Residuals after subtracting the Gaussian.

a) UBVRI Photometry

Most of these data have been previously reported (Paper I) and include results from three observing runs; 1984 November 20 and 21, 1985 January 20, and 1985 November 13. The latter observations were obtained on the Siding Spring Observatory (SSO) 1.0 m telescope, while the rest were obtained with the SSO 2.3 m telescope. The two-channel chopping photometer (TCC; see Paper I) was used for all the observations. In Table 3 we summarize the observed mean magnitudes and colors, and their values corrected for the adjacent F5 V contaminant star, while in Figure 7 we include the *B* light curves obtained from the *UBVRI* data.

b) High-Speed Photometry

Observations taken in 1985 January 21 and 24 and December 11, 12, 13, 14, and 15 were conducted on the 2.3 m telescope utilizing the TCC in a nonchopping mode. A time resolution of 200 ms was used, and all observations were taken through the *B* filter, except those of 1985 December 11, which were in *V*. These observations were undertaken with the aim of conducting a time series analysis on the light curves, and hence no correction was made for extinction. A total of 23.5 hr of high-speed photometry was collected on 1H0542−407, with an average of 3.5 hr per night. We include these data in Figure 7. Note that the high-speed data are in units of raw counts and are uncorrected for sky, which was always at a level of less than 10%, usually at ∼7%.

c) Time Series Analysis

A time series analysis on all our photometry was undertaken with the aim of investigating the periodicities which might be present, specifically the rotation, orbital and sideband (beat) periods. The same period searching techniques described in § IIc were employed, with the DFT method utilized in a manner which allowed successive prewhitening of sinusoidal

TABLE 3

MAGNITUDES AND COLORS OF THE 1H0542 − 407 SYSTEM

Magnitude/ Color	1H0542−407 + Adjacent Star	Adjacent F5 V	1H0542−407
V	14.9	15.9	15.7
U−*B*	−0.95	0.03	−1.39
B−*V*	0.30	0.45	0.15
V−*R*	0.40	0.28	0.52
V−*I*	0.70	0.53	0.86
V−*J*	0.93	0.83	1.03
V−*H*	1.36	1.06	1.62
V−*K*	1.72	1.10	2.15

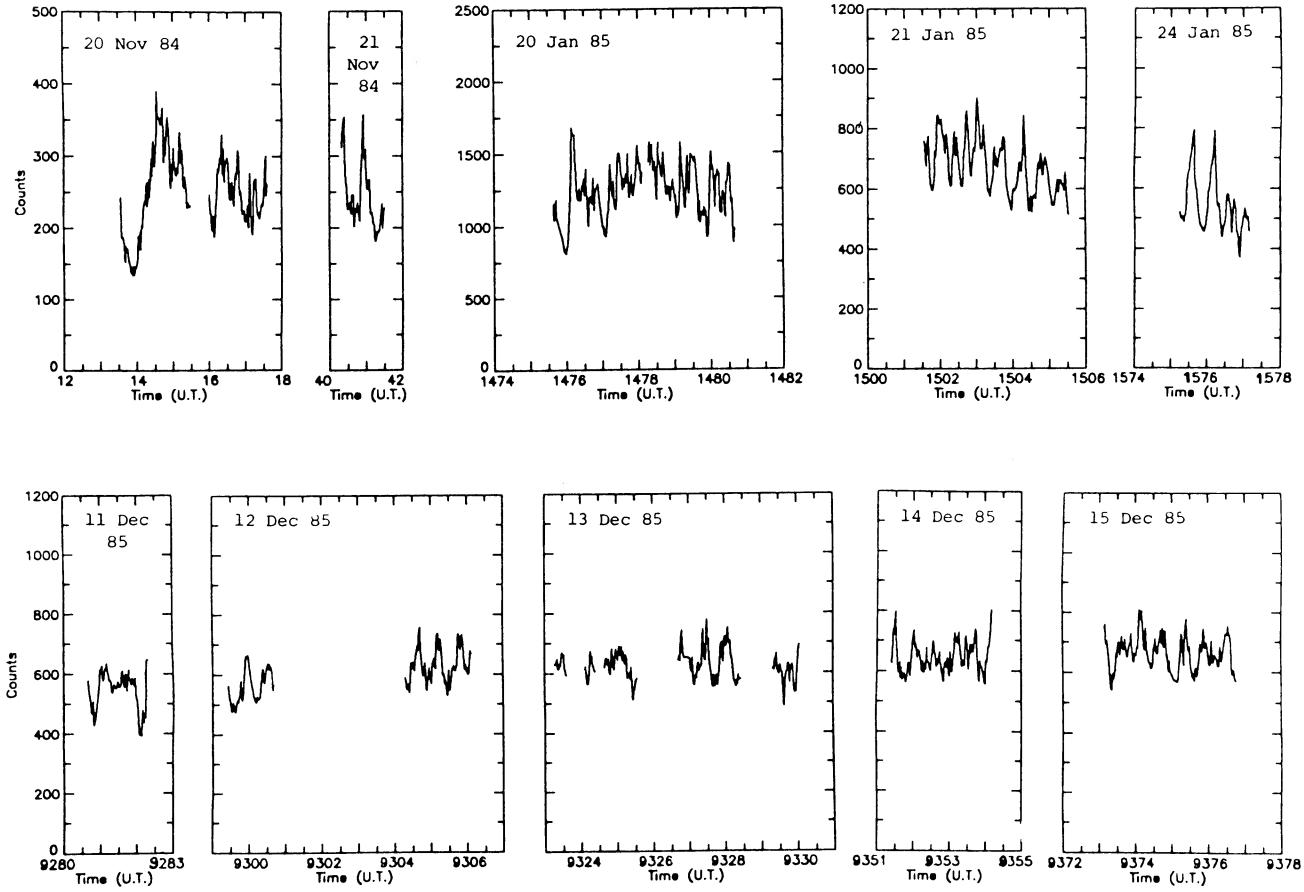

FIG. 7.—The complete *B*-band photometry (except 1985 December 11, which is *V*) of 1H0542−407 taken from 1984 November to 1985 December. Times are UT hours since the first observations on 1985 January 21.

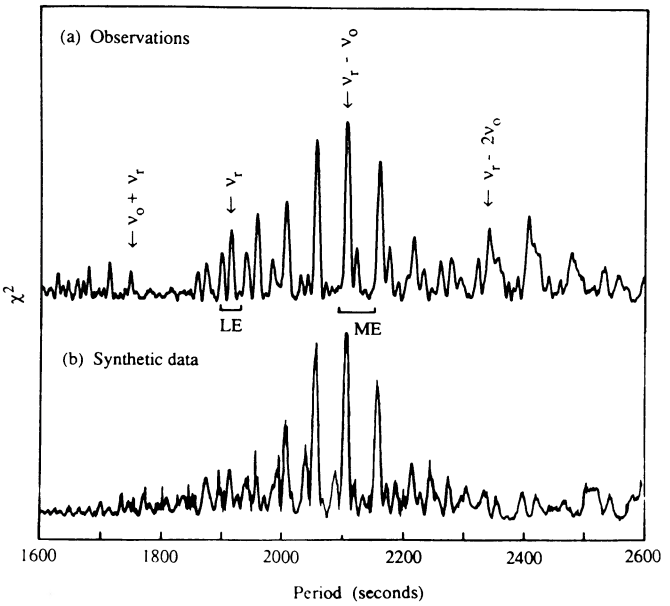

FIG. 8.—Periodograms, derived using the period-folding technique. (*a*) Photometry taken on 1985 December 11–15; ν_r is the rotation frequency, and ν_0 is the orbital frequency. The expected sideband frequencies are marked with arrows, while bars indicate the X-ray periodicities obtained with the low-energy telescope (LE) and medium-energy array (ME) on *EXOSAT* (Tuohy *et al.* 1986). (*b*) Synthesized light curves with sinusoidal period of 2106 s sampled in the same manner as the observations and with Poisson noise added.

periodicities. In Figures 8*a* and 9 we show the periodogram, derived using the epoch-folding and DFT methods, respectively, for the five nights of data collected in the 1985 December run. The window functions indicate the presence of pseudo-periodicities introduced by the unequal data sampling. In Figure 8*a* we have marked the X-ray periodicities determined in Paper I, plus the spectroscopically determined white dwarf rotation period. Clearly obvious are the one-day alias peaks. When the two nights in 1985 January are included in the analysis, each individual peak seen in Figures 8*a* and 9 is split into fine-alias structure corresponding to a frequency of one cycle in ~320 days, the latter being the separation of the two observing runs. The dominant optical periodicity (initially ~2106 s) was successively prewhitened from the data before repeating the DFT analysis. In Table 4 we summarize the results and list the periods, amplitudes, and phases for the strongest periods.

The prewhitening DFT code was used on the two sets of *UBVRI* data: the 1984 November and 1985 January runs. In the latter we found the dominant period to be 2108 ± 9 s, while in the former the dominant period was 2340 ± 10 s.

d) Sideband Periods

A common feature of the DQ Her stars is an optical periodicity at the beat frequency given by $\nu_{\rm rotation} - \nu_{\rm orbital}$. This beat period is, in fact, the dominant optical periodicity in the systems V1223 Sgr and AO Psc. Such periodicities may arise

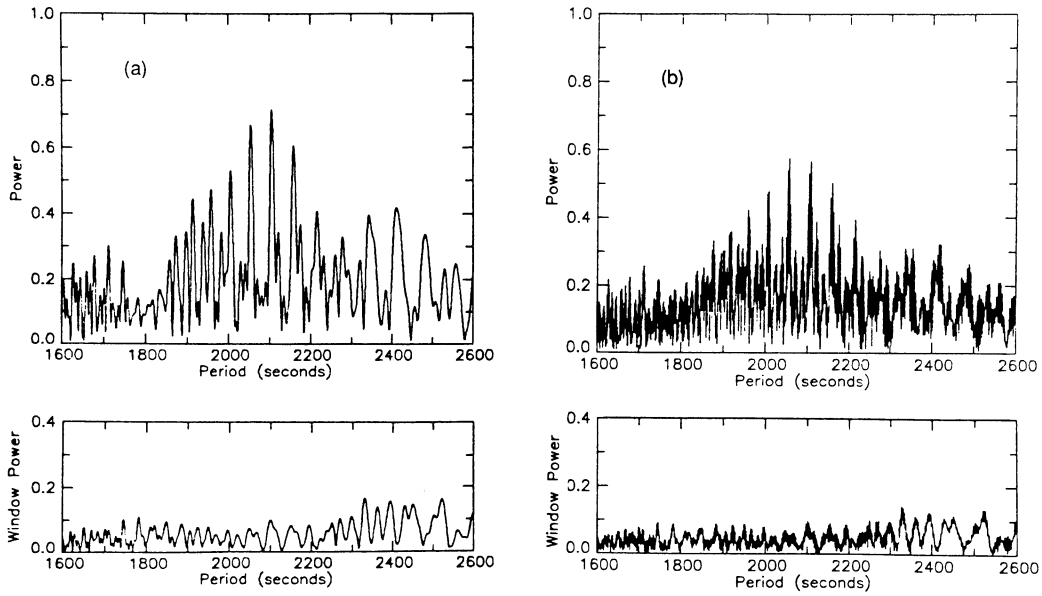

FIG. 9.—Periodograms derived using the discrete Fourier transform method. (*a*) Photometry taken on 1985 December 11–15. (*b*) Entire photometry data set, including *B*-band data from TCC runs (1984 November and 1985 January) and all the high-speed photometry (1985 January and December).

from reprocessing of X-rays, beamed from the white dwarf magnetic poles, in parts of the binary system rotating at $v_{\rm orbital}$. Such sites include the secondary star (Patterson and Price 1981) and/or the hot-spot/bulge in the accretion disk where the stream of material from the secondary impacts the disk (Hassall *et al.* 1981; Wickramasinghe, Stobie, and Bessell 1982). In a recent paper, Warner (1986) showed that one can expect multiple sidebands in DQ Her systems arising from various modulation mechanisms. Some of these include disk obscuration effects and reflection phenomena. Warner showed that a Fourier analysis of light curves exhibiting all the expected behavior should identify variations at the following frequencies: $\nu_r - 2\nu_0$, $\nu_r - \nu_0$, ν and $\nu_r + \nu_0$, where ν_r is the white dwarf rotation frequency and ν_0 is the orbital frequency. We have already shown that our spectroscopic and X-ray results point to a white dwarf rotation period of 1908 s and an orbital period of ~5.7 hr. The predicted sideband at $\nu_r - \nu_0$ is therefore ~2103 s. We, in fact, observe the dominant period peak to be 2106.0 ± 1.2 s and therefore adopt this more accurate value as the higher period sideband $\nu_H = \nu - \nu_0$. The lower period sideband, $\nu_L = \nu_r + \nu_0$, is predicted to be at ~1746 s, which is close to an observed peak at 1748.5 ± 1.8 s, which we therefore adopt as ν_L. These observed periods, ν_H and ν_L were then used to improve the accuracy of ν_r and ν_0, by evaluating the sum and difference, respectively. The updated periods are: $P_{\rm rot}\,(\nu_r^{-1}) = 1911 \pm 2$ s (=31.85 ± 0.03 minutes) and $P_{\rm orb}\,(\nu_0^{-1}) = 5.72 \pm 0.07$ hr.

A further prediction can be made for the value of the $\nu_r - 2\nu_0$ sideband (the beating of the beat frequency itself with the orbital frequency), namely 2346.5 s. In our periodograms, we observe a broad period peak at ~2340 s, which we now attribute to a blend of the sideband $\nu_r - 2\nu_0$ and an alias of $\nu_r - \nu_0$. 1H0542−407 therefore joins V1223 Sgr and AO Psc as a system exhibiting its dominant optical periodicity at the beat period and, furthermore, like V1223 Sgr (Warner and Cropper 1984), shows the "beating beat" period ($\nu_r - 2\nu_0$).

Unfortunately a one-day alias of the $\nu_r - \nu_0$ sideband occurs at ~1911 s, which makes it difficult to observe a period at ν_r. Even prewhitening the $\nu_r - \nu_0$ sideband does not fully remove its influence, since the variation is not purely sinusoidal. We therefore cannot say that there is evidence in these data for optical variations at the rotation period of the white dwarf. However, such variations cannot be ruled out, although they must be below the level of the three most significant periods ($\nu_r - 2\nu_0$, $\nu_r - \nu_0$, and $\nu_r + \nu_0$) in the present data. This result is not entirely incompatible with the conclusions of Paper I in

TABLE 4

ELEMENTS OF THE OPTICAL AND X-RAY LIGHT CURVES

Light Curve	Frequency	Period (s)	$T_{\rm max}$ (JD −2,440,000)	Power	Pulse Fraction
B	$\nu - \omega$	2106.0 ± 1.4	6411.3301	0.64	7.5%
	$\nu - 2\omega$	2350.2 ± 2.8	6411.3457	0.27	4.3
	$\nu + \omega$	1748.3 ± 1.0	6411.2702	0.22	2.6
LE	ν	1918.7 ± 7.8	6119.6838	0.66	75
	$\nu - \omega$	2100.9 ± 11.4	6119.6984	0.30	25
ME	ν	1903.2 ± 7.2	6119.6848	0.38	13
	$\nu - \omega$	2118.3 ± 11	6119.6994	0.56	15

which we claimed that the *UBVRI* photometry showed evidence of a 1980 s peak. That epoch-folding analysis was carried out using data from a single night at a time, rather than a summed data set. Hence the period peak is very broad, extending as far as 2106 s. In Figure 8*a* we have identified the positions of all the orbital sidebands.

We subsequently generated a synthetic light curve consisting of a sinusoid, with Poisson noise added, of period 2106 s and semiamplitude of ~8%, sampled in an identical manner to the observations. The periodogram of this light curve is shown in Figure 8*b* and confirms that the strongest peaks seen in the real data are due to this period, and the other sidebands seen are unlikely to be artifacts or aliases.

e) Light Curves

Figure 10 displays all our high-speed photometry, together with the dominant optical sinusoid derived from our DFT analysis, at a period of 2106 s. The folded, prewhitened light curves are displayed in Figures 11*a*, 11*b*, and 11*c*. The ephemerides of these light curves are given in Table 4.

f) Infrared Photometry

Infrared *J*, *H*, and *K* magnitudes of 1H0542−407 were obtained on the AAT Infrared Photometry System on 1988 March 5 to enable us to search for evidence of the secondary star and to investigate the system's flux in the IR. Table 3 includes these *J*, *H*, and *K* measurements and values deconvolved for the effects of the adjacent contaminant star (see § V*i*[i]). This was achieved assuming the star was a $V \sim 15.6$ F5 dwarf with standard colors (Allen 1973; Bessell 1979; Bessell and Brett 1988).

IV. X-RAY OBSERVATIONS

In Paper I we presented the results of our time series analysis of the X-ray light curves that we obtained with *EXOSAT*. The major results were that the dominant periodicity in the softer (0.1–1 keV) LE1 data was at 1920 ± 20 s, identified as the white dwarf rotation period. However, for the harder (1–10 keV) ME light curve, we found the dominant period to be 2100 ± 50 s; i.e., at the reprocessing period. Both light curves showed secondary period peaks at the position of the other's dominant period. We have since undertaken a more detailed analysis of these data using the prewhitening discrete Fourier transform code described in § III*c*. This enabled us to derive amplitudes, phases, and periods for the dominant periodicities in each light curve. Our results essentially confirm those in Paper I, and in Table 4 we include the ephemerides for the two periods, which we identify as the rotation and reprocessing periods.

V. INTERPRETATION AND MODELS

a) Mass Function and Orbital Parameters

The semiamplitude orbital velocity amplitude, $K_1 = 51 \pm 3$ km s^{-1}, and the orbital period, $P_{orb} = 5.72$ hr, were used with Kepler's law to derive the mass function:

$$f(M_2) = \frac{P_{orb} K_1^3}{2\pi G} = \frac{(M_2 \sin i)^3}{(M_1 + M_2)^2} = 3.3 \pm 0.6 \times 10^{-3}\ M_\odot \quad (1)$$

Here we have assumed that the orbital variation of the emission-line velocities reflects the motion of an accretion disk, possibly truncated, symmetrically surrounding the white dwarf. The velocities therefore reflect the primary's motion about the system's center of mass. Notwithstanding the comments of Robinson (1987), we are reasonably confident in the mass function determination. We have shown that unlike many other systems, which show complicated emission-line velocity behavior (e.g., Shafter 1983, 1985; Shafter and Targon 1982), the emission lines in 1H0542−407 are *relatively* uncomplicated in that the *K*-velocity does not vary as a function of the line width; i.e., the core and wing orbital velocity variations are the same.

Next we invoke the well-established, albeit empirical, secondary mass-period relations for cataclysmic variables (Faulkner 1971; Patterson 1984), which implies a secondary star mass of $M_2 \sim 0.63\ M_\odot$ and $0.57\ M_\odot$, respectively.

If we treat the white dwarf mass as a free parameter, such that $M_1 < 1.4\ M_\odot$, then we arrive at the conclusion that 1H0542−407 has an inclination $i < 25°$. In Figure 12 we show a diagnostic diagram of mass contours for various values of the orbital inclination. Other aspects of this figure are alluded to in future sections. In Table 5 we present the orbital parameters for several assumed white dwarf masses.

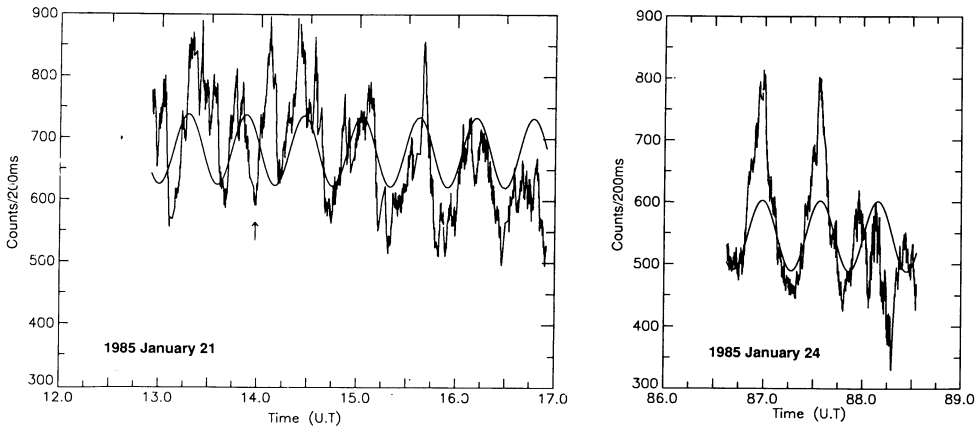

FIG. 10.—The 1985 December high-speed photometry plotted with the 2106 s beat period modulation. The same phase reference (at maximum light) applies to all the separate nights and is given in Table 3.

b) Mass Transfer Rates

The mass transfer rate is one of the most important, and, at the same time, uncertain parameters to be determined in a cataclysmic variable (CV). We have determined values for this parameter based on several sources: the original magnetic braking theory of Verbunt and Zwaan (1981), Patterson's (1984) rotational braking model, and the conservative magnetic braking theory of Rappaport, Verbunt, and Joss (1983) discussed by Lamb and Melia (1987). The latter authors have shown this to produce realistic rates of mass transfer for the longer period systems as well as a period gap similar to that observed. We used their Figure 3 to derive a value of between 3 and 5×10^{16} g s^{-1}. The estimates based on all three theories are shown in Table 6, with all of them less than the critical upper limit of $\gtrsim 5 \times 10^{17}$ g s^{-1} for $M_1 \gtrsim 1\ M_\odot$ for erupting dwarf novae (Shafter, Wheeler, and Cannizzo 1986). Another DQ Her system similar to 1H0542−407, TV Col, has a comparable orbital period (5.49 hr) and a $\dot{M}$ of $\sim 10^{17}$ g s^{-1} (Mouchet *et al.* 1981).

c) Rotational Velocities

i) *The Rotation-Illumination Model*

In Penning's (1985) discussion of the four long-period DQ Her systems (V1223 Sgr, AO Psc, FO Aqr, and BG CMi), he attributes the observed short-period velocity excursions, which he convincingly shows occur at the white dwarf spin period, to an illuminated spot on the accretion disk. In his model, an area of the disk is illuminated by a beam of X-rays from the white

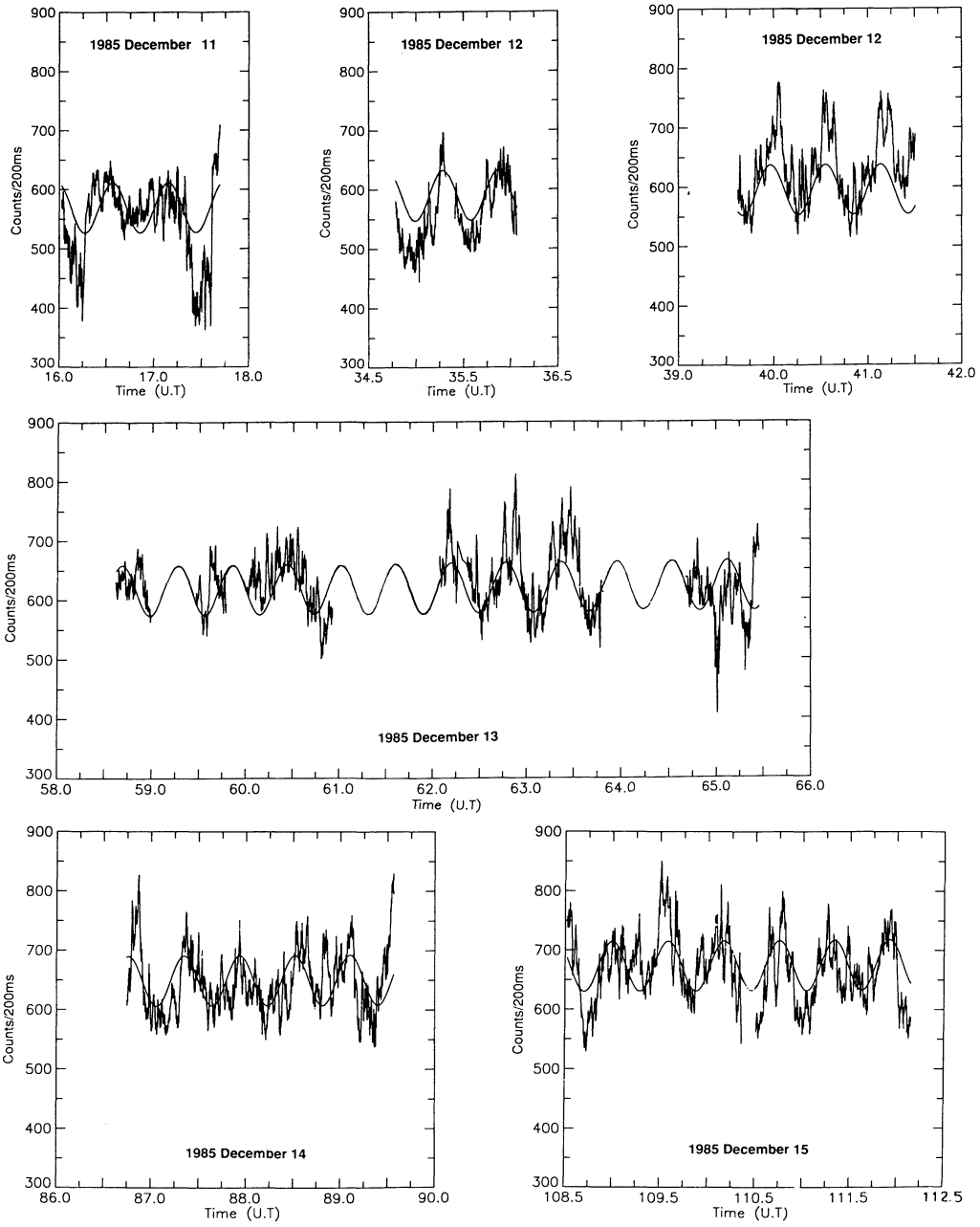

FIG. 10—*continued*

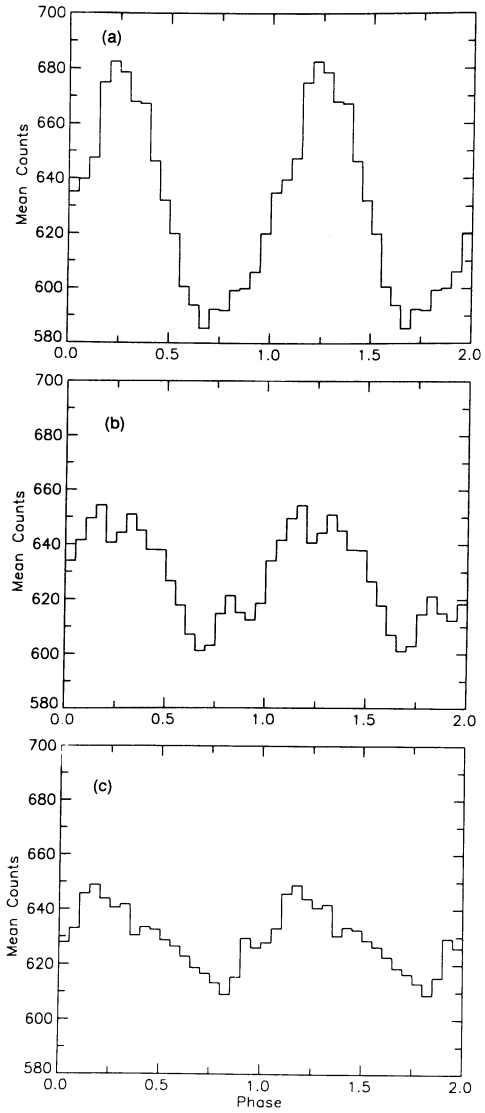

FIG. 11.—*B*-band photometry folded at (*a*) the 2106 s beat ($v - \omega$), or reprocessing, period. (*b*) The $v - 2\omega$ (2345 s) sideband period, after prewhitening of the $v - \omega$ period. (*c*) The $v + \omega$ (1748 s) sideband period, after prewhitening of the $v - \omega$ and $v - 2\omega$ periods. Two cycles are shown. Ephemerides are given in Table 4.

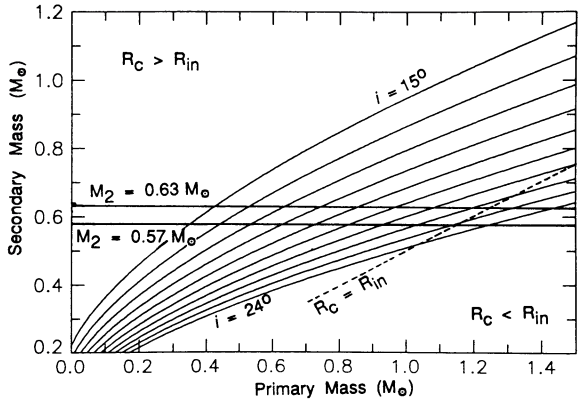

FIG. 12.—Diagnostic diagram for the masses of the component stars of 1H0542−407, assuming a K_1 velocity of 51 km s^{-1} and orbital period 5.72 hr. The inclination contours are shown for $i < 25°$. The two heavy horizontal lines at $M_2 = 0.57$ and 0.63 are the mass estimates using Patterson's (1984) and Faulkner's (1971) relations, respectively. The dashed diagonal line segregates the regions $R_{in} < R_c$ and $R_{in} > R_c$, where R_{in} is the inner disk radius and R_c the magnetospheric corotation radius.

dwarf pole(s). The reprocessed optical emission from this region therefore adds to the total luminosity of the disk and, furthermore, the emission lines from this spot will have a velocity reflecting the mean Keplerian motion of material in the spot. As the illuminating beam sweeps around the disk, this velocity will be seen to vary at the white dwarf spin period. We have investigated this model for 1H0542−407 in which we hypothesize that the short-period velocity variation is due to this mechanism. We calculate the distance this spot has to be from the white dwarf such that its Keplerian velocity equals the observed semivelocity amplitude of the short-period variation:

$$R_{\rm spot} = \frac{GM_1 \sin^2 i}{K_2^2}. \quad (2)$$

Our results show that $R_{\rm spot} \gtrsim a$, the binary separation, for an observed K_2 of ~20–30 km s^{-1} and for $M_1 < 1.4\ M_\odot$. Increasing the azimuthal extent of the spot region could decrease $R_{\rm spot}$; such an increase in the beam would also increase the radial extent and therefore add brighter, faster moving material in the inner disk region to the "spot" with a resultant r^2 increase in the velocity. We are therefore forced to conclude that the rotation-illumination model is incapable of explaining the short-period velocity variations in 1H0542−407. We make further comments on this model in § VI*a*.

ii) *Corotating Magnetosphere Model*

Many of the currently accepted models for DQ Her binaries involve an accretion disk disrupted by magnetic forces at some radius, R_m. These models are qualitatively similar to those of the low-mass X-ray binaries where the neutron star's magnetic field disrupts a disk (e.g., Anzer and Börner 1980, 1983). Quantitatively, the real difference between these models for the white

TABLE 5

1H0542−407 BINARY MODEL PARAMETERS

M_{wd} ($M_\odot$)	R_{wd}[a] (km)	i	q	a (km)	R_{L1} (km)	R_c (km)	R_{inner} (km)	μ_{33} (G cm^3)	B (MG)
1.4.....	1500	24°.2	0.41	1.41×10^6	6.5×10^5	1.48×10^4	1.72×10^4	0.081	24
1.3.....	2900	23.4	0.44	1.39×10^6	6.3×10^5	1.53×10^4	1.50×10^4	0.063	2.6
1.2.....	3850	22.5	0.48	1.36×10^6	6.0×10^5	1.59×10^4	1.28×10^4	0.047	0.82
1.0.....	5500	20.6	0.57	1.31×10^6	5.6×10^5	1.72×10^4	9.11×10^3	0.025	0.15
0.7.....	7800	17.8	0.81	1.22×10^6	4.9×10^5	1.99×10^4	4.79×10^3	0.007	0.02

[a] Assuming Nauenberg's 1972 mass-radius formula.

TABLE 6

MASS TRANSFER RATES FOR 1H0542−407

White Dwarf Mass ($M_\odot$)	Patterson (1984) (g s^{-1})	Verbunt and Zwaan (1981) (g s^{-1})	Lamb and Melia (1987) (g s^{-1})
1.4.....	2.3×10^{17}	1.4×10^{17}	3.0×10^{16}
1.0.....	3.5×10^{17}	2.4×10^{17}	4.9×10^{16}

dwarfs and neutron stars, is the value of the "fastness" parameter. This is the ratio of the Keplerian period of the innermost disk material to the spin period of the star. The neutron star magnetospheres are rotating faster than the inner disk regions, while in the case of white dwarf, they are usually slower rotators (Lamb 1983).

Hameury, King, and Lasota (1986) argue that for systems with orbital periods less than ~ 5 hr, a stable accretion disk cannot form because of this disruption. In their model, the stream of material from the secondary star forms a shock at $\sim R_m$ and proceeds to break up due to both Kelvin-Helmholtz and Rayleigh-Taylor instabilities, forming diamagnetic "blobs" which eventually accrete along field lines. From evolutionary arguments, they further argue that the magnetic moments of the DQ Her systems cannot be too different from the AM Her systems, namely of the order of $\sim 10^{33}$ G cm^3. This view is challenged (e.g., Lamb and Patterson 1983; Lamb 1983; Lamb and Melia 1987) partly on the grounds that there is no evidence of surface magnetic field strengths typical of AM Her systems, namely $B \sim 20$–40 MG.

We have initially adopted the premise that an accretion disk, possibly truncated, is present in 1H0542−407. We now investigate the possibility that the rotationally modulated velocities arise from material forced to corotate in the magnetosphere of the white dwarf. The distance from the white dwarf at which this material exhibits a velocity semiamplitude, K_2, is given by

$$R_c \approx \frac{K_2 P_{\rm rot}}{2\pi \sin i} . \quad (3)$$

The values of R_c range from $\sim 10R_1$ down to $\sim 2R_1$ for white dwarf masses between 1.4 and 0.3 $M_\odot$. Throughout this paper we have used Nauenberg's (1972) white dwarf mass-radius relation.

d) Evidence for an Accretion Disk: Line Profiles

We now ask whether the observed emission line widths can at least be qualitatively explained in terms of a truncated accretion disk model. If we assume that the disk is disrupted at some radius $R_{\rm in}$, then the FWZI of the emission lines produced in the disk are related to the maximum Keplerian velocity at $R_{\rm in}$ (e.g., Wade 1985):

$$R_{\rm in} \approx \frac{4GM_1 \sin^2 i}{({\rm FWZI})^2} . \quad (4)$$

We have already shown that the Balmer lines consist of a narrow and broad component, whereas the He II λ4686 line consists only of the narrower component. In the previous section we have identified the region responsible for the He II, and the narrower Balmer emission, to be somewhere in the white dwarf's magnetosphere. We associated the broad component of the Balmer emission with the truncated disk. This broad component has a FWZI of ~ 2800 km s^{-1}. It is now possible to investigate the range in $R_{\rm in}$ for various values of white dwarf mass and inclination. In Figure 13 we present a diagnostic diagram to illustrate the variation in $R_{\rm in}$. In the same diagram we also show the variation of R_c, the corotation radius of the material producing the narrower emission, as a function of the same parameters. It is clear that we require the condition that $R_c < R_{\rm in}$ for there to be material lost from the disk at its inner radius and then trapped in the star's magnetosphere. We must at this stage emphasize that the derivation of the FWZI is somewhat subjective, depending on how far the wings of the lines extend. Nevertheless, we conclude that only for relatively high white dwarf masses ($M_1 \gtrsim 1\ M_\odot$) is the condition $R_{\rm in} \geq R_c$ met for acceptable values of i. Finally we show the line $R_{\rm in} = R_c$ in Figure 12 and the two regions corresponding to the inequalities $R_{\rm in} < R_c$ and $R_{\rm in} > R_c$, the latter region being the allowable domain for our model for 1H0542−407. In Table 5 we include the parameter values for the system derived in the preceding sections. Our conclusion that the broader Balmer component is produced by the accretion disk is at variance with our preliminary analysis (Buckley and Tuohy 1987). The reason for this was an initial overestimate of the FWZI and the inherent simplistic assumptions equating this value to the maximum velocity attained in the disk.

To investigate the truncated disk model in a more thorough manner, we have adopted the "standard" optically thick accretion disk model to see if it can qualitatively, or even quantitatively, explain the line profiles of the broad component. Our synthetic line profiles are similar to those used by Shafter, Szkody, and Thorstensen (1986) and Horne and Marsh (1986). An axisymmetric disk with a standard radial power-law intensity variation was assumed, with the disk material exhibiting pure Keplerian motion about the white dwarf. Furthermore, the emission-line profile from a disk area element was assumed to be Gaussian, with a dispersion pro-

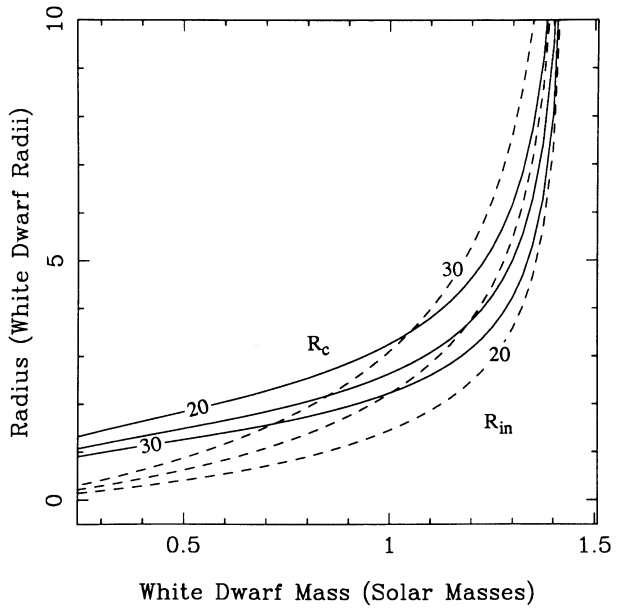

FIG. 13.—Diagnostic diagram for the inner disk radius, $R_{\rm in}$ (*dashed lines*), and magnetospheric corotation radius, R_c (*solid lines*), based on eqs. (5.6) and (5.7), adopting $K_2 \sim 20$ km s^{-1}, $P_{\rm spin} = 1911$ s, and FWZI ~ 2800 km s^{-1}. Contours are for inclinations of 20°, 25°, and 30°.

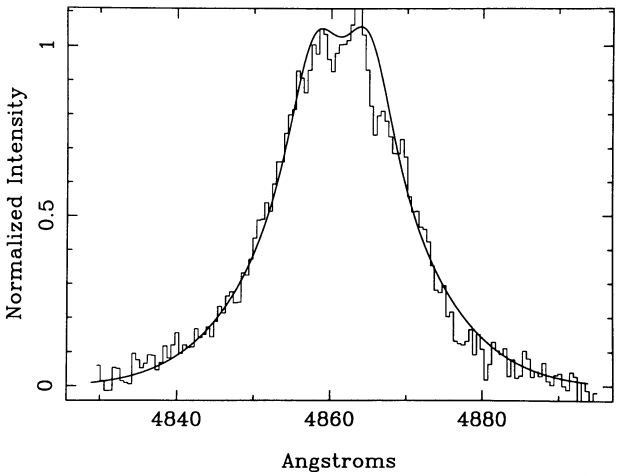

FIG. 14.—Synthetic Hβ emission line profile predicted by our model (§§ Vc, g), based on a standard power-law accretion disk and plotted with a representative observed profile of the broad Hβ component. The parameter values were $i = 25°$, $M_1 = 1.3\ M_\odot$, $R_{in} = 7\ R_1$, $R_{out} = 195\ R_1$, $\alpha = 2.2$, $\sigma = 0.2$.

portional to its Keplerian velocity, V_K. We have not attempted to iteratively fit a synthetic profile to our data; rather we have experimented by changing the values of the parameters after initially setting the inner and outer radii (R_{in}, R_{out}), the inclination (i), and white dwarf mass (M_1) according to our model discussed above. The specific intensity is assumed to vary as $r^{-\alpha}$. Horne and Marsh (1986) show that in the wings of an accretion disk profile, the intensity of the profile should vary as a function of velocity in the following manner:

$$I \propto V^{(2\alpha - 5)} \quad \text{or} \quad \log I \propto (2\alpha - 5) \log V\ . \tag{5}$$

For the wings we obtain $\alpha \sim 2$ and use this as a starting point in our modeling. Furthermore, we adopt a local dispersion of $\sigma = 0.1$–$0.25 V_K$, a value typical of turbulent accretion disks (Shafter, Szkody, and Thorstensen 1986).

In Figure 14 we show a synthetic profile that we were able to obtain with reasonable values (i.e., not *too* different from the values obtained above) of the main parameters (R_{in}, R_{out}, i, M_1). Also plotted in Figure 14 is the observed mean broad Hβ profile, corrected for orbital motion, obtained from the binned spectra (§ II*d*). The best-fit values are $i = 25°$, $M_1 = 1.3\ M_\odot$, $R_{in} = 7\ R_1$, $R_{out} = 195\ R_1$, $\alpha = 2.2$, $\sigma = 0.2$. The overall agreement was excellent considering that the model itself is very simple and that the parameters were determined independently of the model.

Warner (1973) has found an interesting correlation between the quantity $K_1/v_d \sin i$ and the mass ratio, q, where $v_d \sin i$ is the projected rotational velocity of the disk, which takes the form

$$\frac{K_1}{v_d \sin i} = q(0.5 - 0.227 \log q)^2\ . \tag{6}$$

The value of $v_d \sin i$ was taken to be ~(FWHM)/2 of the profile. An improvement on the technique by Shafter (1983, 1985) found that, on average, the full width of the line at ~0.3 times its maximum corresponded to $2v_d \sin i$. We have used this method and derive $v_d \sin i$ to be ~570–740 km s^{-1}, depending on exactly where we place the continuum. This gives a value of $K_1/v_d \sin i$ between ~0.07 and 0.10, implying $q = 0.15$–0.25. This is clearly incompatible with our previous spectroscopic determination of $q \sim 0.5$. If q were indeed ~0.25, this would require the secondary star to be much less massive than expected from the orbital period (i.e., at ~0.3 $M_\odot$). We must at this stage state that we are attempting a determination of q via a calibration which is designed for systems with complete accretion disks as opposed to truncated ones, as proposed here. Given the individual scatter of calibration points plus the possibility of additional complexities in the line profile (e.g., residual magnetospheric component, we consider that the determination of q from this method must necessarily be subject to greater error than the orbital determination in § V*a*.

e) X-Ray Spin Period Modulation: Accretion Column Model

The dominant periodicity of the LE1 light curve is the rotation period of the white dwarf. This is the defining characteristic of the intermediate polars; i.e., the X-ray–emitting DQ Her systems (Warner 1983, 1985). In the standard model for an accretion column (e.g., Lamb 1985; Frank, King, and Raine 1985), material accretes along the magnetic field lines onto the magnetic pole(s) of the white dwarf. The exact accretion regime (AM Her or DQ Her) depends upon the magnetic field strength, mass transfer rate, and white dwarf mass.

For the DQ Her stars, the field lines do not trap the accreted matter at such large distances as for the AM Her stars (i.e., near the secondary star or the stream), and the azimuthal extent of the region threaded by the field, $\Delta\phi$, is considerably larger in the case of disk accretion. This leads to accretion over a much larger area of the white dwarf than in an AM Her system, and also a more complex geometry than cylindrical; for example, the area accreting is likely to be arc or crescent shaped. King and Shaviv (1984) explain the quasi-sinusoidal rotational X-ray light curves of DQ Her systems in terms of occultations of these areas (partial or total) by the body of the white dwarf as it spins. The sinusoidal nature of the lower energy X-ray light curves led these authors to conclude that the fractional areas were of the order $f \sim 0.1$. The light curve shapes, with nearly sinusoidal oscillations for the softer X-rays and square wavelike light curves for the harder X-rays, have been explained in terms of a larger effective area (f) for the lower energies. This occultation model has been challenged by Rosen, Mason, and Córdova (1988), who point out that such a model predicts that the amplitude of the light curves should be essentially independent of energy, contrary to most observations of DQ Her systems. Another serious criticism is the assumption that accretion occurs over the *whole* polecap area, implying that all field lines intersecting the disk trap material and feed it onto the white dwarf. Since the magnetic forces are proportional to r^{-3}, the magnetic disruption of material is expected to occur over a limited range of radii Δr, where $\Delta r \sim r/3 \sim \nabla B/B$, leading to a latitude band rather than polecap accretion region (e.g., Cropper 1986; Rosen, Mason, and Córdova 1988).

We initially adopt the accretion column model of Imamura and Durisen (1983), and then expand it to include accretion over a range of magnetic longitude. The aspect angle of the column, α, defined as the angle between the line of sight and the column is expressed as

$$\alpha = \cos^{-1}(\cos\theta_c \cos i + \sin\theta_c \sin i \cos\phi_{rot})\ , \tag{7}$$

where θ_c is the colatitude of the column (the angle between the spin axis and the accretion column), i is the orbital inclination, and ϕ_{rot} the rotation phase angle ($\phi_{rot} = 0.0$ when the column points closest to the line of sight). The geometry is shown in

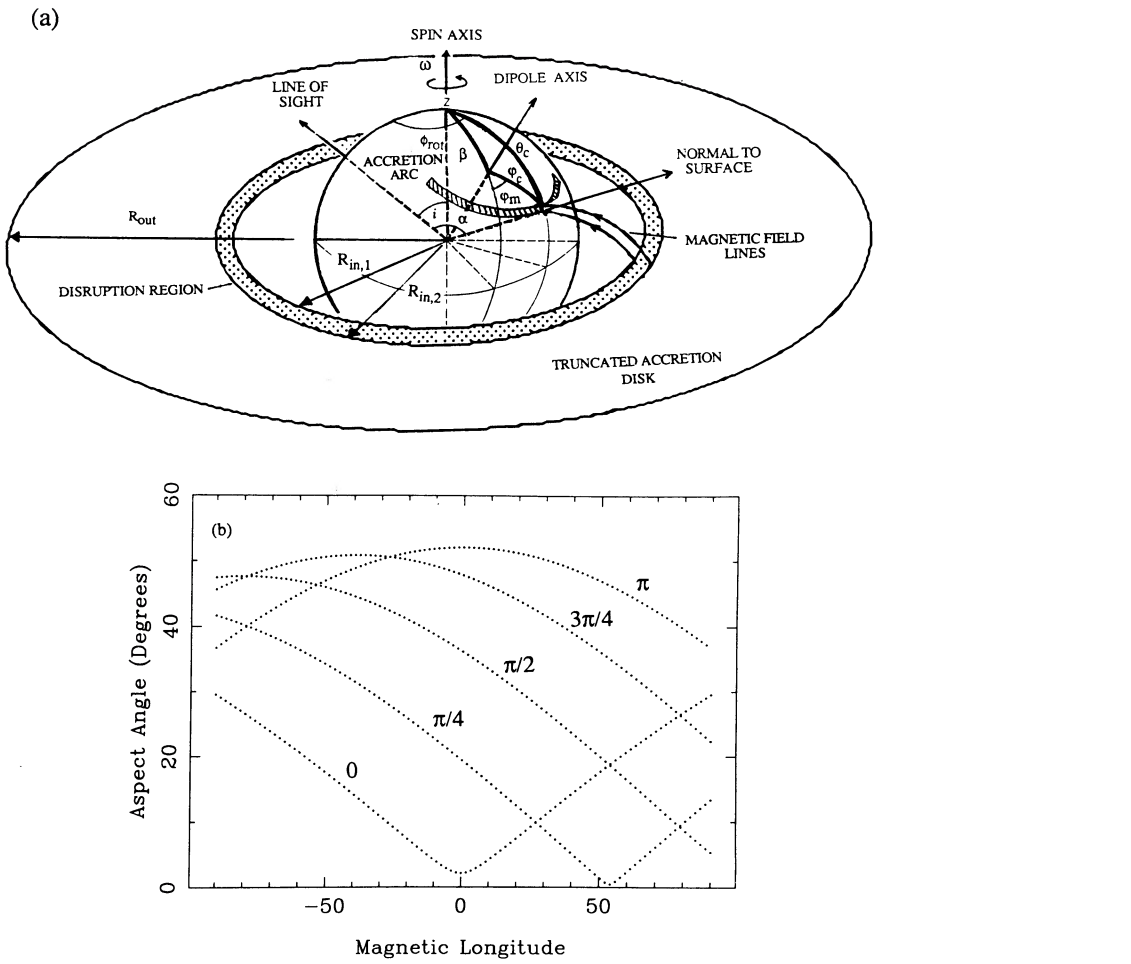

FIG. 15.—(*a*) Accretion geometry for 1H0542−407; α is the aspect angle of the "curtain," β is the dipole tilt angle, φ_c is the magnetic colatitude of column/curtain, φ_m is the magnitude longitude, $R_{\rm in,1}$ and $R_{\rm in,2}$ are the range of radii over which the accretion disk is disrupted. (*b*) Variation in aspect angle, α, between the line of sight and normal to white dwarf surface at φ_c as a function of magnetic longitude for rotation phases 0, $\pi/4$, $\pi/2$, $3\pi/4$, and π.

Figure 15*a*. Wickramasinghe (1988) shows that the *magnetic* colatitude of the column is given by

$$\sin \varphi_c = (R_{\rm in})^{-0.5} \cos \beta (1 - \sin^2 \beta \sin^2 \varphi_m)^{-0.5}, \quad (8)$$

where $R_{\rm in}$ is measured in white dwarf radii, β is the dipole offset angle from the spin axis, and φ_m is the magnetic longitude. The dependence on φ_m implies that accretion will occur at the footprints of the magnetic field lines which intersect the disk over φ_m roughly equal to $-90°$ to $+90°$. These footprints define an arc-shaped area on the white dwarf's surface. $R_{\rm in}$ was determined in § V*d* to be $\sim 7\ R_1$, which leads to φ_c in the range $\sim 15°$–$22°$ for $\beta < 45°$. As $\beta \to 0$, $\varphi_c \to 22°$ and is almost independent of φ_m (or $\phi_{\rm rot}$). The accretion geometry is therefore not so much a column, but rather something analogous to an auroral arc or curtain (e.g., Rosen, Mason, and Córdova 1988). The requirement that we observe the accretion along, rather than perpendicular, to field lines leads us to adopt a small dipole offset of $\beta \sim 5°$, and hence the accretion arc is at a magnetic colatitude of $\sim 22°$. With $i \sim 25°$, the aspect angle α therefore varies from $\sim 2°$ to $50°$ over the rotation cycle for this geometry (Fig. 15*b*). Thus there is no self-eclipse of the emission region and emission from the second pole is never seen. This assumes that the shock height is small ($h \ll R_1$) which we soon show is indeed the case. The model is essentially that used by Rosen, Mason, and Córdova (1988) to explain the marked energy-dependent rotational X-ray modulation in EX Hya, with the exception that emission from both poles is observed in this higher inclination system ($i \sim 78°$).

If the accretion curtain has a magnetic colatitude $\varphi_c(r)$, then accretion from $r = R_{\rm in,1}$ to $R_{\rm in,2}$ will result in a fractional area, f, given approximately as

$$f \sim \frac{\cos [\phi_c(R_{\rm in,2})] - \cos [\phi_c(R_{\rm in,1})]}{2} \frac{\Delta\phi_m}{2\pi} \quad (9)$$

for one pole only. If $\Delta r \sim r/3$, then accretion is expected to occur over a region from ~ 7 to $10\ R_1$, and hence for a small dipole tilt (which we show below is likely), the value of f for each polar accretion region is ~ 0.0025 to 0.005 for $\Delta\phi_m \sim \pi/2$ to π rad.

In Paper I we showed that the LE1 data were modulated at a level of 80%–100% at the spin period compared to $\sim 20\%$–40% for the ME data. Our prewhitening DFT results (§ IV) essentially confirm those of Paper I. These results seem to be incompatible with a self-occultation of the white dwarf hot spot region. The energy dependence of the modulation is compatible with an absorption effect, for example photoelectric

absorption, which affects the lower energy soft X-rays (0.1–2 keV) preferentially.

Theoretical light curves and X-ray spectra based on absorption effects within an accretion column have been produced by Imamura and Durisen (1983). The only significant source of opacity for the bremsstrahlung photons in the hot ($T \gtrsim 10^8$ K) postshock region is electron scattering, which under certain circumstances (e.g., higher accretion rates and/or lower fractional areas) may be highly direction dependent (Lamb 1985; King and Shaviv 1984; Imamura and Durisen 1983), resulting in nonisotropic hard X-ray emission. Imamura and Durisen include the effects of scattering in the ionized, funneled preshock flow, which they maintain is completely ionized in the region immediately above the shock, where the bulk of the Compton scatterings occur. They go on to show that the ratio of the electron scattering optical depths perpendicular and parallel to the field lines is given as

$$\tau_\perp/\tau_\parallel = 0.95(f/0.1)^{0.5}\,, \tag{10}$$

which implies $\tau_\parallel$ is $\sim$5–7 times $\tau_\perp$. Adopting Imamura and Durisen's (1983) formulae for the optical depth across the column leads to values in the range of $\tau_\perp \sim 0.3$–0.4 for $\dot{M} \sim 2 \times 10^{17}$ g s^{-1}, $M_1 \sim 1.3\ M_\odot$. The converging nature of the accretion curtain, compared to the cylindrical column, will increase the effect of scattering the X-rays out of the sides of the curtain. We therefore expect that the X-ray emission will be in the form of a rotating fan beam, with the peak intensity nearly perpendicular to the column. The model regimes of Imamura and Durisen (1983), for $f \sim 0.005$, were investigated in an effort to explain the shape of the rotational hard X-ray light curve quantitatively. Their models were used to parameterize the quantities $\tau_\perp$, $\tau_\parallel$, $kT_{\rm brem}$, $kT_{\rm bb}$, h_s, (shock height), and the luminosities above and below 2 keV (L_h and L_s) in terms of the accretion luminosity ($L_{\rm acc} = GM\dot{M}/R$), which for 1H0542−407 is $\sim 1.2 \times 10^{35}$ ergs s^{-1} or $\sim 0.6 \times 10^{35}$ ergs s^{-1} over each pole. In Table 7 we present the model parameters derived for this accretion luminosity.

TABLE 7

ACCRETION COLUMN PARAMETERS FOR 1H0542−407

Adopted Values	
f	0.005
$\dot{M}$	2×10^{17} g s^{-1}
M_1	$1.3\ M_\odot$
$L_{\rm acc}$	1.2×10^{35} ergs s^{-1}
$kT_{\rm brem}$	$\sim$20 keV
$kT_{\rm bb}$	$\sim$45 eV
L_h	$\sim 2 \times 10^{34}$ ergs s^{-1}
L_s	$\sim 1 \times 10^{35}$ ergs s^{-1}
L (2–10 keV)	$\sim 1 \times 10^{34}$ ergs s^{-1}
L (0.1–2 keV)	$\sim 1 \times 10^{35}$ ergs s^{-1}
h_s (R_1)	$\sim$0.07
$\tau_\parallel$	2.7
$\tau_\perp$	0.4
$N_{\rm H}$	3×10^{21} cm^{-2}
Predicted Fluxes	
F (2–10 keV)	3.3×10^{-11} ergs s^{-1}
F (0.1–2 keV)	8.1×10^{-12} ergs s^{-1}
Observed Fluxes	
F (2–10 keV)	3.3×10^{-11} ergs s^{-1}
F (0.1–2 keV)	7.6×10^{-12} ergs s^{-1}

We now address the predictions of this model. The ratio of the hard X-ray flux escaping the sides of the column to that escaping along it is given as

$$I_\perp = I_\parallel\, e^{-(\tau_\perp - \tau_\parallel)} \sim I_\parallel\, e^{2.3} \sim 10 I_\parallel\,. \tag{11}$$

Hence only $\sim$10% of the flux escaping to infinity perpendicular to the column escapes parallel to it. To achieve the observed $\sim$20% modulation of the directly observed hard (>2 keV) X-rays emitted from the accretion column only requires a change in the line of sight opacity of $\sim$0.2.

We argue that to have the reflected X-ray signal overwhelm the direct signal requires the observed column opacity to be high (i.e., $\gtrsim$2.5), which implies that the column must always be viewed close to parallel.

The morphology of the hard X-ray light curve in 1H0542−407 depends not only upon how α varies with $\phi_{\rm rot}$, but also the functional form of $\tau(\alpha)$. Imamura and Durisen (1983) show that the specific intensity of the hard X-rays is a strong function of μ ($=\cos\alpha$) whenever electron scattering is an important source of opacity. Thus for all rotational phases we expect to be in the moderately high optical depth regime as far as line of sight opacities is concerned for 1H0542−407.

It has been argued (King and Shaviv 1984; Lamb 1985) that if electron scattering opacity is significant in producing nonisotropic emission above 2 keV, then photoabsorption of lower energy photons in the cold, partially ionized preshock plasma is even more important. Lamb (1985) concludes that if the viewing angle of the column is $\lesssim 30°$, then photoabsorption will produce a significantly deeper minimum for the softer X-rays. This is exactly what is observed; the LE1 (0.1–2 keV) light curve is modulated at 80%–100%.

The model we adopt, based on Imamura and Durisen (1983), has a significant soft X-ray luminosity ($\sim$5 times the hard bremsstrahlung luminosity), which is partly due to energy deposited at the white dwarf surface (mainly via hard bremsstrahlung photons and Comptonized electrons) and reradiated as a blackbody of $kT_{\rm bb} \sim 45$ eV. This blackbody emission will occur in and around where the column meets the white dwarf surface and have a Lambertian (i.e., limb-darkened) distribution, ignoring absorption effects. At rotational phases when we view this region through the partially ionized column of accreting material, the photoelectric absorption optical depth is very large. At phases when the column points away from the line of sight, the soft X-rays are much less obscured by the column, and those emitted in the region around it escape through a significantly reduced optical depth. The *EXOSAT* observations reported in Paper I were described by a simple bremsstrahlung model with a moderately high column of $\sim 10^{21}$ H cm^{-2}. This result is certainly compatible with our model, since the column density must be dominated by absorption within the system, because interstellar absorption is negligible at the galactic latitude for 1H0542−407 of 35°.

We now ask whether our accretion column model is compatible with the observed *EXOSAT* fluxes. Bremsstrahlung and blackbody spectra were calculated with $kT = 20$ keV and 45 eV, respectively, and initially zero absorption. The normalizations were then adjusted so that (1) the ratio of the flux below 2 keV to that above was $\sim$5 (the ratio of the luminosities in the model) and (2) the 2–10 keV flux equaled that observed, namely 3.3×10^{-11} ergs cm^{-2} s^{-1}. Finally, these spectra were subjected to observing columns between 1×10^{21} and 3×10^{21} H cm^{-2}, the latter being an upper limit from Paper I. In Table 7 we present the predicted fluxes in the 0.1–2

keV and 2–10 keV bands and compare them to the observed values derived in Paper I. The 0.1–2 keV flux is the sum of both the bremsstrahlung and blackbody components, while the 2–10 keV flux is entirely dominated by bremsstrahlung emission. Only for the upper limit for the absorbing column are we able to say that the model and observations are compatible. Of course, the true picture is more complex than the adopted model and is likely to be $\dot{M}$, and hence time, dependent. Variations in the parameters L_{acc} and f will change the energy budget and the opacity of the column. However, we require at least that the optical depth to electron scattering be high enough to account for preferential absorption along the line of sight so that the reflected hard X-ray signal dominates over the direct (see also § Vf). This requirement means that L_{acc}/f must be a reasonably high number, of the order $\sim 10^{36}$ ergs s^{-1}.

Finally, we make a comment concerning the possible presence of the Fe Kα emission line. In Paper I we identified this line in our *EXOSAT* spectrum with an equivalent width of $\sim$0.4 keV. The strength of this line is in the range expected of an accretion column with $\tau_\perp \sim 0.2$–1.0 (Swank, Fabian, and Ross 1984).

f) The X-Ray Beat Period: Reflection

We concluded in § III*d* that the dominant optical periodicity arose from reprocessing of X-rays at a point fixed in the binary frame of reference, probably either the secondary star or the bulge in the disk. A simple and analogous explanation of the X-ray variability seen at this same period is the reflection of X-rays from this same region, which we now investigate.

X-ray reflection has been studied by several authors including Basko and Sunyaev (1973), Basko, Sunyaev, and Titarchuk (1974), Milgrom and Salpeter (1975*a*, *b*), and Felsteiner and Opher (1976). The interaction of X-rays with the surface of a normal star produces a stellar wind effect in which the outflowing gas is heated to high temperatures by the hard X-rays. An increased mass outflow can result if there is an appreciable soft X-ray flux which decreases the height of the transition region (Basko and Sunyaev 1973). A consequence of this wind was shown by Basko, Sunyaev, and Titarchuk (1974) to be increased albedo of the star to softer X-rays in the range $\sim$3–10 keV. The reflected X-rays are emitted in a nonisotropic manner with harder X-rays preferentially reflected at $\sim 90°$ to the normal incidence flux. Furthermore, the energy albedo is greater for higher angles of incidence. Approximately 30%–40% of the incident X-ray flux is reflected, while the rest is absorbed and heats the atmosphere which reradiates as an approximate blackbody in the optical/UV region.

We therefore have a mechanism which is able to modulate the hard (ME) X-ray emission at the *beat* period, namely X-ray reflection. Degradation of the energies of the reflected photons, through Compton scattering in the hot wind/corona, may account for the weak second period peak observed at the beat period in the LE1 data.

We now address whether the observed pulse amplitude of $\sim$20% can be explained in terms of the current model, at least qualitatively. If we adopt the arguments of Wickramasinghe, Stobie, and Bessell (1982), then for *isotropic* X-ray emission over 2π sr, the accretion disk and secondary will intercept up to 7% and 3% of the X-ray flux, respectively. Since the hard X-ray emission is far from isotropic, it is possible that the interception percentages could be increased by a factor of 5. The reflected X-rays themselves are also not isotropically reemitted, but the emission pattern is dependent both on photon energy and the angle of incidence (e.g., Basko and Sunyaev 1973; Milgrom and Salpeter 1975*a*; Felsteiner and Opher 1976); indeed, the problem is a rather complex one. By invoking beaming to reduce the direct line-of-sight X-ray flux from the white dwarf to $\sim$10% of the flux sweeping the disk/secondary star, plus nonisotropic reflection off the secondary, we are able to obtain pulse fractions as large as $\sim$30%. We have assumed that, due to its symmetry, the disk does not modulate the reflected X-ray signal; however, in principle we might expect a spin modulation to arise from changes in the angle between the line of sight and reflection vectors. We have also neglected the disk hot spot, which would increase the modulation at the reprocessing period. Our conclusion is that the observed $\sim$30% hard X-ray modulation at the beat period is consistent with reflection off the secondary.

g) The Optical Beat Period: X-Ray Reprocessing Model

In order to investigate the X-ray reprocessing we have developed the following model which incorporates X-ray irradiation of an accretion disk, its hotspot, and the inner facing surface of the secondary star.

i) *The Accretion Disk*

The standard optically thick α-accretion disk model of Shakura and Sunyaev (1973) was adopted, with an adaptation which restricted the disk to a minimum radius, R_{in}, equal to the magnetospheric radius. We used the following expression for central disk temperature ($z = 0.0$) T_0, height H, and optical depth τ as a function of radius (Frank, King, and Raine 1985):

$$T_0(R) = 1.4 \times 10^4 \alpha^{-0.2} \dot{M}_{16}^{0.3} M_1^{0.25} R_{10}^{-0.75} r^{1.2} \text{ K} , \quad (12)$$

$$H(R) = 1.7 \times 10^8 \alpha^{0.1} \dot{M}_{16}^{0.15} M_1^{-0.375} R_{10}^{1.125} r^{0.6} \text{ cm} , \quad (13)$$

$$\tau(R) = 33 \alpha^{-0.8} \dot{M}_{16}^{0.2} r^{0.8} , \quad (14)$$

where $r = 1 - (R_{in}/R)^{0.5}$ and the *surface* temperature of the disk is given as

$$T(R, H) \approx T_0(R) \tau^{-0.25} \text{ K} . \quad (15)$$

The nature of most parameters is self-evident, with the subscripts defining the units (e.g., $\dot{M}_{16}$ is in 10^{16} g s^{-1}, M_1 is in solar masses, and R_{10} in 10^{10} cm).

The disk spectrum was then calculated by integrating the Planckian flux of individual annuli of constant radius over the whole disk:

$$F_\lambda = \int_{R_{in}}^{R_{out}} 2\pi B_\lambda [T_{eff}(R)] R \, dR . \quad (16)$$

The size of the disk is specified by the outer and inner radii. We adopted the previous estimates of R_{in}, where the spin period velocity variations are interpreted in terms of a magnetospheric disruption model (§ V*c*[ii]). As for the outer radius, Shafter (1983) shows that if the transferred material conserves angular momentum, the outer radius of an inviscid disk is

$$r_J = a(1 + q)[0.5 - 0.227 \log q]^4 . \quad (17)$$

In the real world of the viscous disk, momentum is transferred outward so that the outer disk radius is expected to be larger. From observations of many CVs (e.g., Hessman 1988; Sulkanen, Brasure, and Patterson 1981; Shafter 1983) a typical outer disk radius is $\sim 2.5 r_J$, which we have used.

We have treated the X-ray irradiation of the disk in the following manner. First, we assume that the X-rays emanate

TABLE 8

PARAMETERS FOR ACCRETION DISK, HOT SPOT, AND SECONDARY STAR

i	25°
M_1	1.3 $M_\odot$
R_{in}	7 R_1
R_{out}	195 R_1
R_{hs}	180 R_1
d_{hs}	15 R_1
α	0.5
F_D	0.25
L_X	2.5×10^{34} ergs s^{-1}
$\dot{M}$	7.5×10^{16} g s^{-1}
$h(R_{out})$	5.2 R_1
h(hs)	~ 5 R_1

from a point source at a height above the $z = 0$ disk plane of $h_X \sim \cos(\varphi_c + \beta)$ white dwarf radii. The X-rays are confined to a fan beam with an azimuthal extent of $2\pi f_D$ rad. For each disk annulus of constant R, the angle of incidence of the X-rays is calculated. We assume that $\sim 60\%$ of incident X-rays in the major region of interest (0.1–10 keV) are absorbed and, further, that this energy is reradiated as a blackbody of temperature $T_X(R)$, where

$$T_X(R) = \left[\frac{F_X(R) + \sigma T^4(R)}{\sigma}\right]^{0.25} \text{K}, \quad (18)$$

$F_X(R)$ is the absorbed flux at R, corrected for incidence angle, and $T(R)$ the disk temperature before X-ray irradiation. A correction factor of cos i was finally applied to the emergent line-of-sight flux to account for disk inclination. The parameters, and their likely values, for the disk model are given in Table 8.

ii) *The Hot Spot/Bulge*

One of the possible sites for X-ray reprocessing giving rise to an optical modulation at the beat period is the disk hot spot or bulge (Hassall *et al.* 1981; Wickramasinghe, Stobie, and Bessell 1982). We have added a simple circular hot spot to our disk model, based upon the work of Bath *et al.* (1974). The temperature of the hot spot is T_{hs}, vertical thickness h_{hs}, and radius d_{hs}. The total area of the spot is thus $\sim L_{hs}/\sigma T_{hs}^4 \sim \pi d_{hs}^2$, where L_{hs} is the spot luminosity. We have used the expressions given by Bath *et al.* (1974) for each of these quantities.

iii) *The Secondary Star*

The only other significant reprocessing site is the heated face of the secondary star (e.g., Patterson and Price 1981). For the purposes of our model we have assumed the secondary to be spherical with a radius equal to the mean Roche lobe radius (Eggleton 1983),

$$R_2 = a\left[\frac{0.49q^{2/3}}{0.6q^{2/3} + \ln(1 + q^{1/3})}\right]. \quad (19)$$

We deduce a secondary spectral type of M0 V and effective temperature of ~ 3800 K based on the empirical ZAMS calibration for other CVs (Patterson 1984). The secondary hemisphere facing the white dwarf was divided up into a series of annular areas about the line of centers of the stars. Each annulus has a constant X-ray angle of incidence and therefore X-ray–modified effective temperature. We use equation (18) to calculate the temperature after irradiation. For a low inclination angle ($i < 25°$), the projected area of the secondary star thus consisted of a major contribution ($> 50\%$) from the unilluminated side and the remainder from the heated surface. We note that a typical disk thickness at R_{out} is ~ 5 R_1, and hence the half angle which the disk subtends is $\lesssim 1.^\circ 5$ compared to $\sim 20°$ for the Roche lobe filling secondary. Shadowing of the secondary by the outer disk is therefore considered to be less important than, for example, in AO Psc (Wickramasinghe, Stobie, and Bessell 1982). This effect has therefore been neglected in our model.

iv) *Reprocessing Model Results*

The above integrated model for reprocessing in the accretion disk, hot spot, and secondary was used to synthesize the overall flux distribution from the various components. These results were compared to the observed continuum flux distribution and were used to predict the optical pulse amplitudes arising from reprocessing. The disk parameters were in turn used in the accretion disk profile simulation code (§ V*d*) to check consistency. We held constant the parameters $\alpha = 0.5$, $i = 25°$, $h_X = 0.7$ and varied the following within the limits $1.0 < M_1 < 1.4$, $5 < \dot{M}_{16} < 15$, $3 < R_{in,\,wd} < 12$, $0.25 < f_d < 0.5$, $1 < L_{X,34} < 10$. We define $R_{out} = \sim 2.5 r_J$ (eq. [17]) and assumed $R_{hs} = R_{out} - d_{hs}$.

We were able to arrive at a result which adequately accounted for the observations (both the flux distribution and emission line widths) and at the same time is consistent with the dynamical and accretion column models. The result is summarized in Table 8, and the flux distributions for the various components are shown in Figure 16, while in Figure 17*a* we compare the mean model flux distribution to our only accurately fluxed spectrum (Paper I), and in Figure 17*b* we include the U, B, V, R, I, J, H, and K magnitudes, deconvolved for the effects of the F5 V contaminant star (IIIf). The magnitudes are all displaced by -0.2 in log F_λ for clarity. Over most of the optical to IR wavelength interval, the model distribution agrees quite well with the observations and can be fitted with an $\alpha = -2.4$ power law; i.e., $F_\lambda \propto \lambda^{-2.4}$. This is close to the expected power law for an optically thick, stable accretion disk, namely $\alpha = -2.33$ (Lynden-Bell 1969).

Pertinent points concerning the results of the overall model are now discussed. The system has a rather high white dwarf

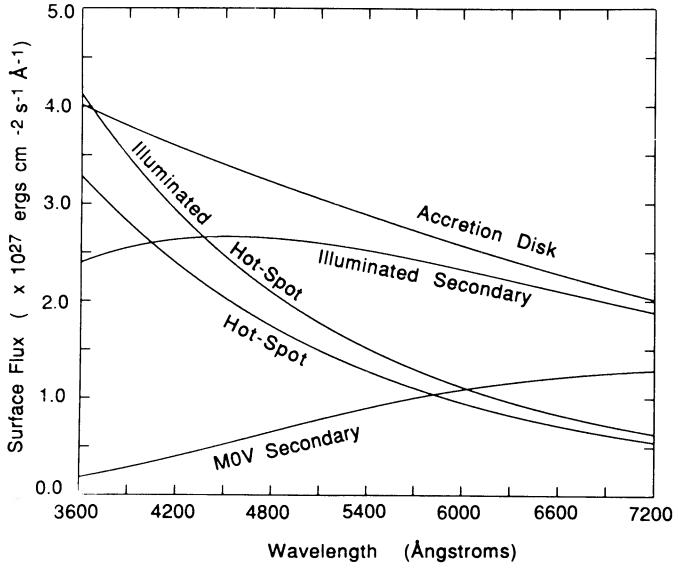

FIG. 16.—Predicted flux distribution from the various components making up the reprocessing model for 1H0542−407 (§§ V*g*, *h*).

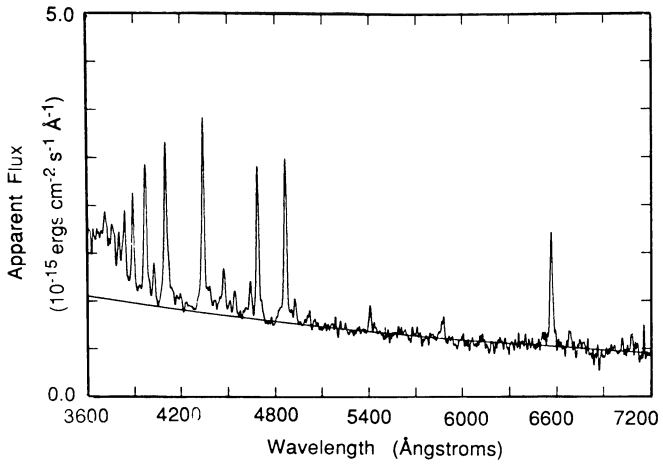

FIG. 17*a*

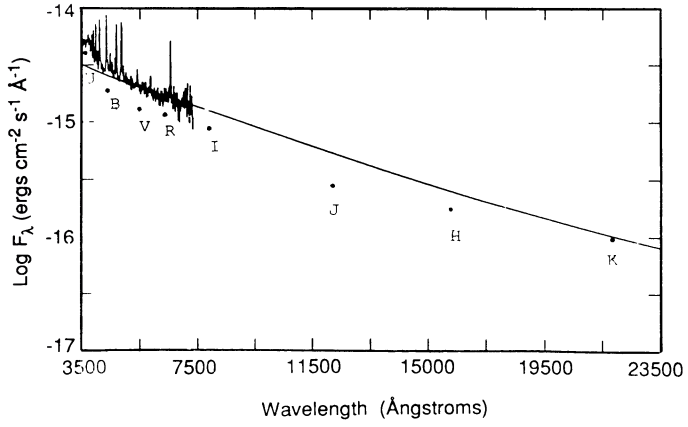

FIG. 17*b*

FIG. 17.—(*a*) The mean summed spectrum of all the components shown in Fig. 15, compared to the observed flux distribution (Paper I), scaled to a distance of ~570 pc. (*b*) Observed magnitudes (displaced by −0.2 in log F_λ for clarity), deconvolved for the effects of contamination by the nearby (~4″) F5 V star, plotted with the observed spectrum and the model flux distribution.

mass ($\sim 1.3\ M_\odot$) and an accretion disk which is mostly intact, being disrupted close to the white dwarf. Any decrease in M_1 has to be offset by a decrease in R_{in}/R_1. However, as this ratio approaches ~3 at $M_1 \sim 0.9\ M_\odot$, the regime changes such that accretion occurs over a much larger area of the white dwarf (Bath *et al.* 1974), and thus $f \gg 0.01$ and L_f ($=L_{acc}/f$) is decreased by an order of magnitude. As our accretion column model (§§ V*e*, *f*) demands $L_f \gtrsim 10^{36}$ ergs s^{-1}, we are forced to consider $R_{in}/R_1 \gtrsim 5$, so that we have a sufficiently small *f*-value. The adopted value for R_{out} of 195 R_1 (5.66×10^{10} cm) implies that the accretion disk extends to ~90% of the mean Roche lobe radius, a value considered typical in CVs (e.g., Shafter, Szkody, and Thorstensen 1986).

The X-ray luminosity of 2.5×10^{34} ergs s^{-1} applies to the magnetic pole we can see and, therefore, implies a total accretion luminosity of $\sim 5 \times 10^{34}$ ergs s^{-1}, although this is likely to be somewhat higher to account for opacity effects plus the disk luminosity. The total accretion luminosity is thus up to half that assumed for the accretion column model in § V*e*. However, note that such a variation is observationally supported by the existence of brighter states of presumed enhanced mass transfer (e.g., in 1988 March). It is therefore possible that 1H0542−407 was in a somewhat brighter (by ~1 mag) state of enhanced mass transfer during the *EXOSAT* observations.

The spot bolometric luminosity is $\sim 1.2 \times 10^{33}$ ergs s^{-1} and is a dominant contributor to the total blueward flux; i.e., at $\lambda \lesssim 3600$ Å. Its height is $\sim 5\ R_1$, of the order of the disk thickness, and its radius is $\sim 15\ R_1$. Therefore the angle subtended by the hot spot at the white dwarf surface is $\sim 2d_{hs}/R_{hs}$ radians, or ~9°. This is somewhat less than the typical 20° (Bath *et al.* 1974) inferred from eclipse observations of CVs with humps (e.g., Warner 1974). However, these systems (e.g., SU UMa binaries) are shorter period, smaller disk systems with hot spots subtending commensurably larger angles.

The secondary star's atmosphere reaches a maximum temperature due to irradiation, at the sub–X-ray point of ~8500 K which falls off to the ambient temperature of ~3800 K at the terminator. We note, however, that in our simplified spherical geometry we have neglected the effects of gravity darkening, which will tend to increase the temperature of the polar region and decrease the equatorial temperatures of a Roche lobe filling secondary.

We see that the mean flux distribution well represents the observed continuum over the interval $\lambda\lambda$3900–7400. The additional continuum flux observed blueward of $\sim\lambda$3900 is in part due to the Balmer jump in emission, arising from the optically thin region of the disk. This region is the hot "chromosphere" of the disk which we have not attempted to model here. Additional contributions to the system luminosity, particularly in the UV, may also be expected from the disk/magnetosphere interface where it is expected oblique Kelvin-Helmholtz shocks may form.

By fixing the disk parameters to those derived above (i.e., in Table 8), we were able to achieve a reasonable accretion disk model line profile, which matches the observations, by adjusting the power-law exponent (§ V*d*) to equal −2.2, the result of which is shown in Figure 14 for the Hβ line. This value of α is certainly in the range expected for our Shakura-Sunyaev disk model, which predicts a shallower falloff in intensity for the inner disk regions and a steeper value further out than a constant power law does.

h) Optical Modulation Amplitudes

A question which must now be addressed is whether the observed amplitudes of the optical modulations can be adequately explained in terms of the proposed reprocessing model. White and Marshall (1981) concluded that for AO Psc, the ratio of reprocessed optical flux to X-ray flux was much larger than expected from a simple reprocessing of isotropically emitted X-rays. A similar situation exists for other DQ Her systems; for instance, FO Aqr has an X-ray flux which is 1/10 that required (Patterson and Steiner 1983). Several solutions to this dilemma have been proposed, including X-ray beaming (Warner 1985) and the presence of another component to the beamed luminosity; e.g., a soft X-ray flux. Our model for 1H0542−407 has both these effects, a fan beam and increased soft X-rays from Compton scattering within an accretion curtain with significant electron scattering opacity.

i) *The White Dwarf Spin Period*

In general, we expect any reprocessed optical luminosity from an accretion disk to be modulated at the white dwarf spin period. Such an effect is due to the concave disk surface which produces a front-back asymmetry (Cropper 1986). Wickramasinghe, Stobie, and Bessell (1982) find that the amplitude

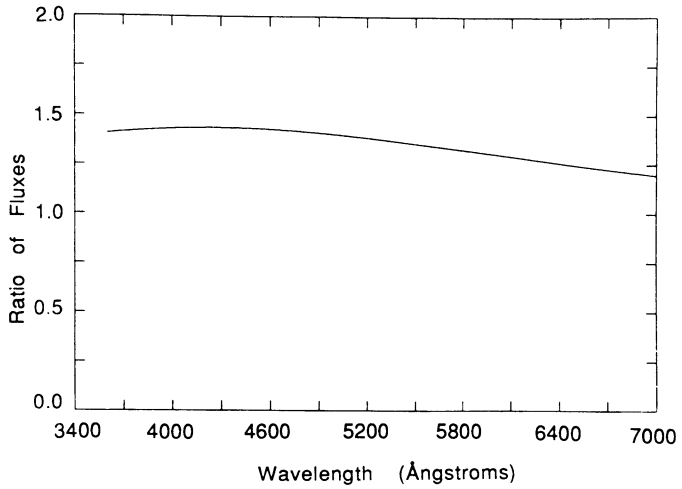

FIG. 18.—Ratio of X-ray illuminated to non-illuminated fluxes for the reprocessing model (§§V*g*, *h*).

of such a variation is $\sim \tan i \tan \delta$, where δ is the maximum angular extent in the z-direction of the disk as seen from the white dwarf. Our α-disk model predicts $\delta \sim 3°$, and, with $i \sim 25°$, the rotationally modulated reprocessed flux should have an amplitude $\lesssim 2\%$. Additional unmodulated flux will dilute this modulation even further. We note that the upper limit derived for the spin modulation is $\sim 2.5\%$.

ii) *Reprocessed Modulation*

In Figure 18 we present the ratio of the spectra for the models with and without X-ray illumination. This represents the maximum full-amplitude flux variation as a function of wavelength and ranges from 44% in the blue to 21% in the red, which corresponds to pulse fractions of 22% to 11%. Additional sources of optical flux (or a Rayleigh-Jeans tail of an EUV/UV source), not so far considered, could reduce these pulse fractions. Such a source could be the accretion column/curtain, the hot spot on the white dwarf, or the magnetospheric disruption region. Our *UBVRI* photometry (Paper I and § III*a*) give pulse fractions from 14% (*U*) to 11% (*R*). The folded light curve for the entire high-speed *B*-band photometry has a pulse fraction of $\sim 8\%$, which corrected for the contaminant star using the procedure outlined in Paper I, is $\sim 17\%$. Considering possible uncertainties arising from the deconvolution process, plus the temporal changes in system luminosity, flickering, etc., the model is quite able to explain the observed pulse fractions.

i) Luminosities and Distances

In Table 9 the surface fluxes and absolute V magnitudes are listed for the three components of the model.

i) *The Secondary Star*

The nonirradiated secondary star has $M_V = 8.95$, which is very close to the predicted value of ~ 9 based upon Patterson's (1984) empirical M_V-period relation. We use Bailey's (1981) method to determine the distance to 1H0542−407 using the IR observations (§ III*f*). We have deconvolved the J, H, and K magnitudes for the effects of contamination by the nearby $V \approx 15.6$ F5 V star, and the corrected values are given in Table 3. The $V-K$ measurement of ~ 2.2 is clearly affected by the disk and hot spot and should not be taken as an indication of the secondary's color. Instead, we adopt a standard $V-K$ of 3.7 for a M0 V star (Bessell and Brett 1988). If we assume all of the K flux ($K \sim 13.6$) comes from the secondary star, then we derive a lower limit to the distance of ~ 450 pc, which varies by less than ± 100 pc over a wide range of $V-K$.

TABLE 9

PREDICTED SURFACE FLUXES AND ABSOLUTE MAGNITUDES OF THE COMPONENTS OF THE MODEL FOR 1H0542−407

Component	F_V (ergs cm s^{-1} Å^{-1})	M_V
Accretion disk	2.83×10^{27}	7.74
M0 V secondary star	9.3×10^{26}	8.95
Disk hot spot	1.2×10^{27}	8.67
Illuminated secondary	2.48×10^{27}	7.88
Illuminated hot spot	1.43×10^{27}	8.48
Sum of rows 1–3 (nonilluminated)	5.02×10^{27}	7.12
Sum of rows 1, 4–5 (illuminated)	6.89×10^{27}	6.78
Mean	5.9×10^{27}	6.94

ii) M_V *of the Disk*

Here we use Patterson's (1984) calibration between the Hβ equivalent width and $M_{V,\mathrm{disk}}$. The broad component of the Balmer line, which we have attributed to the accretion disk, has an E.W. in the range 15–20 Å. Since only the inner, optically thick dominated regions of the disk are absent in our truncated disk model, we can still safely use Patterson's calibration for CVs with normal (i.e., undisrupted) disks. The implied $M_{V,\mathrm{disk}}$ is ~ 7–7.5, contrary to our claim in Paper I of ~ 9. This latter estimate was, however, based on the premise (now shown to be false) that all of the line emission was produced in the disk, whereas we have convincingly shown that a major contribution arises in the magnetosphere. We further note that the model predicts $M_{V,\mathrm{disk}}$ to be ~ 7.7, not too different from the empirical result and certainly in the range expected for dwarf novae in quiescence (Wade 1985).

The model has a total mean M_V of ~ 6.9 which implies a distance of ~ 570 pc for a mean observed V of 15.7.

iii) *X-Ray Models*

The accretion column model described in §§ V*e*, *f* has a 2–10 keV unabsorbed luminosity of $\sim 1 \times 10^{34}$ ergs s^{-1}. If we accept that electron scattering reduces the average line-of-sight flux by a factor ~ 0.1 (i.e., line of sight $\tau_{es} \sim 2.3$), then from the observed 2–10 keV flux of 3.3×10^{-11} ergs cm^{-1} s^{-1}, we derive a lower limit distance of ~ 500 pc. We note that a 2–10 keV luminosity of $\sim 10^{34}$ ergs s^{-1} is near the upper limit for CVs (Córdova and Mason 1983) but is compatible with some upper limits determined in other DQ Her systems (e.g., AO Psc, Hassall *et al.* 1981; Berriman 1988). The higher luminosity is consistent with the high white dwarf mass and increased $\dot{M}$ for the longer orbital period. The conclusion of this section is that several independent lines of inquiry lead to a distance of $\gtrsim 500$ pc for 1H0542−407. Such a value is larger than usually thought for DQ Her binaries; however, in the final section of this paper (§ VI*e*) we discuss the possibility that X-ray luminosities higher than previously thought may explain problems with X-ray reprocessing energetics.

j) Magnetic Fields

The magnetospheric radius has been shown by King, Frank, and Ritter (1985) to be

$$r_\mu = 2.7 \times 10^{10} \mu_{33}^{4/7} \dot{M}_{16}^{-2/7} M_1^{-1/7} \phi \text{ cm} , \qquad (20)$$

where μ_{33} is the magnetic moment (in units of 10^{33} G cm^3) and ϕ is a dimensionless variable dependent upon the accretion geometry, equal to 0.5 for accretion via a disk and 0.37 for diskless accretion as in AM Her systems (King 1985). If we accept that $r_\mu = R_{in} \sim 7\ R_1$ and adopt the standard values ($M_1 = 1.3$, $\dot{M}_{16} = 7.5$, $R_9 = 0.29$), then we derive a field strength of ~ 6 MG. In Figure 19 we show the variation in r_μ with M_1 for several assumed field values and constant $\dot{M}_{16} = 7.5$. If we confine the parameter values (M_1 and r_μ) to those allowable by our above models, then we find that B has to be in the range 1–10 MG. Such values are expected if the DQ Her systems have magnetic moments smaller than the AM Her binaries, all of which have field strengths of between ~ 20 and 60 MG, as is believed to be the case by Lamb (1983, 1985), Lamb and Patterson (1983), Lamb and Melia (1987). Null detections, or low values, of circular polarization in DQ Her systems (e.g., Penning, Schmidt, and Liebert 1986; Cropper 1986; Watts *et al.* 1986), with one exception, seem to lend support to the weaker field hypothesis. Even for the exception, BG CMi, where $\sim 4\%$ circular polarization is detected at H (West, Berriman, and Schmidt 1987), the magnetic field is only 5–10 MG. This is contrary to the ideas of some workers (King, Frank, and Ritter 1985; Hameury, King, and Lasota 1986), who argue that the moments are essentially equal for DQ and AM Her systems. Indeed, Chanmugam and Ray (1984) and Chanmugam and Frank (1987) claim that the low polarization values, or upper limits, do not necessarily imply low field values, a view challenged by Wickramasinghe (1988).

In general, the only reliable estimates of B in DQ Her stars are derived from their equilibrium spin periods (Lamb 1983; Schmidt and Liebert 1987) and rate of change of their spin periods. If the white dwarf is spinning at its equilibrium period, then the total torque acting on the white dwarf vanishes; that is, the accretion torque acting to spin up the star is equal and opposite to the magnetic torque trying to slow it down. King, Frank, and Ritter (1985) show that the following inequality holds:

$$\frac{P_{spin}}{P_{orb}} \geq \frac{P_{eq}}{P_{orb}} = \left(\frac{r_\mu}{a}\right)^{3/2} (1+q)^{1/3} . \quad (21)$$

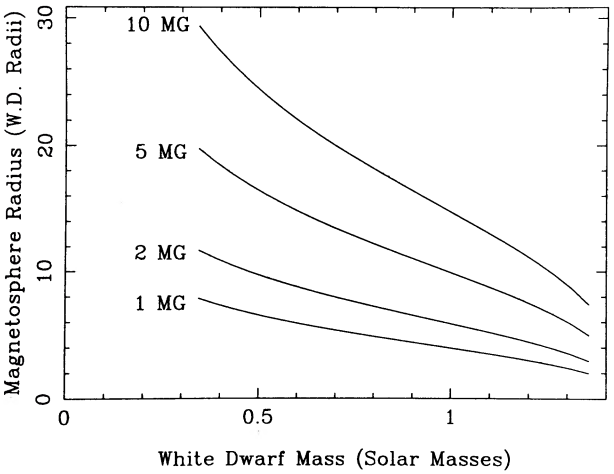

FIG. 19.—Magnetospheric radius as a function of white dwarf mass and parameterized for surface magnetic field strengths of 1, 2, 5, and 10 MG and a mass transfer rate $\dot{M} = 7.5 \times 10^{16}$ g s^{-1} ($1.2 \times 10^{-9}\ M_\odot$ yr^{-1}).

For 1H0542−407, this implies r_μ/a must be less than 0.18, and as $r_\mu/a \sim 0.015$, we conclude that the white dwarf is not spinning at its equilibrium value and predict that $\dot{P}_{spin} < 0$.

VI. DISCUSSION AND COMPARISONS

a) The Illuminated Spot Model

Our conclusion regarding the inapplicability of the rotational illumination model (Penning 1985) as applied to 1H0542−407, and the subsequent explanation of the rotationally modulated velocites in terms of magnetospheric disruption of an accretion disk (§ Vc[i]–[ii]), lead us to reexamine Penning's model in more detail. We pursued a similar analysis on Penning's data for V1223 Sgr and BG CMi (3A0729+103), the two systems with the most complete determination of system parameters. The spin-modulated velocity variations are interpreted in the framework of our magnetospheric disruption model. For V1223 Sgr, the observed velocity semiamplitude is ~ 90 km s^{-1}, and the magnetospheric corotation radius (eq. [3]) is in the range ~ 2.5–5 white dwarf radii (R_1) over the allowable range in inclination (15°–27°; Penning 1985). This is in good agreement with the inner radius of the accretion disk, as deduced from the line widths, which vary from ~ 2.5–6 white dwarf radii over the allowable range in inclination and white dwarf mass (0.4–0.6 $M_\odot$). In the case of BG CMi, the respective ranges are $R_{in} \sim 4$–$20\ R_1$ and $R_c \sim 1.5$–$5\ R_1$, with an overlap of the two near $i \sim 20°$ and $M_1 \sim 1\ M_\odot$, the upper limits given by Penning. We conclude that the velocity variations at the white dwarf spin period seen in 1H0542−407, V1223 Sgr, and BG CMi can all be explained by magnetospheric disruption of an accretion disk and the subsequently trapped material being pulled around by the magnetic field of the white dwarf.

b) Alternative Sideband X-Ray Period Model

An alternative explanation for sideband X-ray periods in DQ Her systems has been offered by Mason, Rosen, and Hellier (1987). Here the mass transfer stream is disrupted by magnetic pressures before it circularizes and forms a disk through viscous stresses. The stream therefore penetrates directly into the magnetosphere at a point of constant azimuth angle, i.e., fixed in the binary frame of reference. As the tilted dipole spins, the accretion rate onto the magnetic pole is modulated, which in turn leads to an X-ray flux variation at the beat period. This is referred to as the "accretion gating" model by Mason (1985) and Lamb and Mason (1988), and has been used to explain the X-ray modulations seen in 1H0542−407 and V1223 Sgr (Mason, Rosen, and Hellier 1987; Lamb and Melia 1987). We have investigated this alternative for 1H0542−407 and conclude below that, except for improbably high magnetic field strengths, it is unlikely to be the mechanism responsible for sideband modulation of the hard X-rays.

Lamb and Melia (1987) show that the magnetic moments (μ) for DQ Her stars are approximately one order of magnitude less than AM Her stars. They further conclude that accretion disks will be present in DQ Her stars of sufficiently low μ. The criterion for the presence of a disk is that $r_J > r_\mu$, namely the radius of an inviscid ring, r_J (eq. [17]), be larger than the magnetosphere. Over a wide range of primary mass (1.4–1.0 $M_\odot$), the radius of such a ring is $\sim 2 \times 10^{10}$ cm. If we equate this with the magnetospheric radius (see eq. [20]), then we derive the following lower limits to the magnetic field strength,

B, of 40–350 MG for a white dwarf mass of 1.0–1.3 $M_\odot$ and a mass transfer rate of 7.5×10^{16} g s^{-1}. This, in turn, implies $\mu \sim 6$–9×10^{33} G cm^3. There is no evidence for such a large surface field, and we restate that the 3 σ upper limit for circular polarization in 1H0542−407 is 1% (Paper I). We also note that even in the model of Hameury, King, and Lasota (1986), accretion disks are expected to be present in DQ Her systems with orbital periods greater than ~5 hr. There is ample evidence in most DQ Her systems for accretion disks, even for those with shorter periods, for example EX Hya (Hellier *et al.* 1987). Such evidence includes the line widths and sometimes the presence of tell-tale double-peaked emission, a recognized signature for an accretion disk.

c) EX Hya: Models for Spin Modulation of Emission Lines

As already stated, the accretion model for EX Hya is quite similar to 1H0542−407 (§ V*e*). The increased inclination of EX Hya (~78°) allows emission regions from both poles to be seen (Kaitchuck *et al.* 1987; Rosen, Mason, and Córdova 1988). While the former authors show that the lines widths are modulated at the 67 m white dwarf spin period, they report no velocity variations at this period. However, the variation in the ratio of the strengths of the red and blue peaks of the line profile over the spin period, reported by Hellier *et al.* (1987), might be interpreted as a velocity variation. If our magnetospheric disruption model can be applied to this system, then for an inner disk radius of ~10 R_1, a white dwarf mass of 0.78 $M_\odot$, and inclination of 78° (Hellier *et al.* 1987), a velocity semiamplitude of ~100 km s^{-1} would be expected at the spin period. The absence of such a velocity to date may be a result of the complex nature of the line profile (e.g., the S-wave) and the close commensurability of the orbital and spin periods (i.e., $P_{\rm spin} = 2/3 P_{\rm orb}$).

The model which Kaitchuck *et al.* (1987) use to explain the line width variations has an accretion funnel over both poles. As the white dwarf rotates, our view of the funnel(s) changes from looking almost along it, to transversely to it. In the former orientation, we observe an increase in the line widths due to material streaming in both (opposed) directions onto the poles. In 1H0542−407, the low value of the observed rotationally modulated velocity, ~30 km s^{-1}, implies that the streaming motions of gas toward the poles must be negligible in the region dominantly responsible for the emission. We have already identified the emission site to be the disk region between $R_{\rm in}$ and $R_{\rm in} + \Delta R$ (see § V*e*), where the field lines thread the disk. Here the gas velocity is dominated by turbulence, a possible result of the shock at $R_{\rm in} = r_\mu$ where the gas is suddenly slowed from Keplerian motion to forced magnetospheric rotation. The emission from this region will dominate over any emission from closer to the poles, where the gas becomes fully ionized. In this picture we do not expect a variation of line width at the spin period. The presence of such a variation may be explained as follows. If there is a component to the emission from gas leaving the disk/magnetosphere region in the form of a wind (e.g., Honeycutt, Schlegel, and Kaitchuck 1986), then the superposition of this component would produce just such a modulation. The wind component would be blueshifted with respect to gas corotating at the disk/magnetosphere boundary. Thus at maximum approach velocity (i.e., blueshift) of this rotating gas, the sum of both components will result in a narrower line than at maximum recessional velocity.

d) TV Col: A Look-alike?

TV Col is the most similar DQ Her system to 1H0542−407 in terms of orbital and spin periods, at 5.49 hr and 1911 s (actually identical to 1H0542−407!), respectively. This system has the added complication of a 5.2 hr beat period attributed to a ~4 day precession of a tilted/warped disk. It is now joined by 1H0542−407 in that both show no sign of a rotational optical variation, and neither does it exhibit an orbital-rotational beat period modulation. Flux measurements from the UV to IR are well fitted by a combination of an optically thick disk spectrum and a ~9000 K blackbody, the latter probably attributable to a disk bulge/hot spot (Mouchet *et al.* 1981). Mouchet *et al.* (1981) further find that the mass transfer rate is $\gtrsim 10^{17}$ g s^{-1}, implying an accretion luminosity of $\sim 10^{35}$ ergs s^{-1}. Recent unpublished IR photometry (Berriman 1988) indicates a distance of $\gtrsim$ 500 pc. Thus we see that TV Col shares several characteristics with 1H0542−407, most importantly, similar accretion parameters and distance. Recently TV Col was observed to undergo a $V \sim 3$–4 mag outburst (Schwarz and Heemskerk 1987), thus joining EX Hya, SW Uma, and GK Per as DQ Her systems exhibiting dwarf nova–like outbursts.

e) AO Psc

We have already discussed this system in § V*e* with regard to X-ray reprocessing sites. The system shows a similar behavior in its X-ray light curves to 1H0542−407 in that the softer energies are more strongly pulsed. Rather than appealing to large polecap fraction (f), as King and Shaviv (1984) do, we prefer to invoke the accretion curtain model (§ V*e*; Rosen, Mason, and Córdova 1988), where accretion occurs over an arc-shaped region on the white dwarf surface of approximately constant magnetic latitude. If we furthermore invoke line-of-sight opacity variations, then pseudo-sinusoidal X-ray modulations are expected. We now make the interesting observation that if the harder X-rays are produced near the center of this arc (where $\dot{M}$ is greatest, and hence $L_{\rm acc}/f$), and the X-rays are fan-beamed, then the brief dip observed in the 5–15 keV light curve (White and Marshall 1981) could be due to the disappearance of part of this hard X-ray–emitting region over the limb of the white dwarf as it rotates. Such a dip would not be seen at lower energies since the emission region is likely to be more extended (e.g., Wickramasinghe 1988).

We now remark on the aforementioned problem with the energetics of X-ray reprocessing (§ V*h*). Our results for 1H0542−407 show that if we invoke optical depth effects, with subsequent beaming, and an increased intrinsic X-ray luminosity and therefore distance, then the deficit between X-ray and reprocessed liminosities seen in AO Psc (White and Marshall 1981) and FO Aqr (Patterson and Steiner 1983) disappears. We note that there is already some evidence for larger distances for DQ Her stars, particularly arguments based upon IR observations of the secondary stars (§ V*i*[i]; and Berriman 1988).

We also comment that the problematic emission-line variations of 1H0542−407 at the spin period are also seen in AO Psc. Wickramasinghe, Stobie, and Bessell (1982) observed a ~25% EW variation for He II λ4686, at the *beat* period. Hutchings and Coté (1986) found velocity variations at $K \sim$ 50 km s^{-1} for He II, Hβ, and He I, which were also modulated at the beat, rather than spin period, although the latter could not be definitely excluded. These results seem to rule out an

X-ray–illuminated inner disk model, like that proposed for DQ Her by Chanan, Nelson, and Margon (1978), since such a model predicts variation only at the spin period. Hutchings and Coté believe an explanation lies in reprocessing off a fixed feature in the binary frame.

Finally, we make the interesting observation that for all of the low inclination ($i \lesssim 30°$) DQ Her systems (V1223 Sgr, AO Psc, and 1H0542−407), the dominant optical variation occurs at the reprocessing period. A natural explanation of this effect may be the lack of front-back disk asymmetry in low inclination systems (see § V*h*[i]), and hence reprocessing off the disk (where the spin-modulated flux arises) produces an essentially constant (i.e., unmodulated) optical flux.

VII. SUMMARY AND CONCLUSIONS

Our model for 1H0542−407 can be summarized as follows. The system is a DQ Herculis binary, or intermediate polar, consisting of a high-mass ($\sim 1.3\ M_\odot$) white dwarf with a spin period of 1911 s in a 5.7 hr orbital period with a $\sim 0.6\ M_\odot$ M0 dwarf secondary. The system is viewed at low inclination ($i \lesssim 25°$), with the result that we observe only one accreting pole. An accretion disk is disrupted by the white dwarf's magnetic field at a distance of $\sim 2 \times 10^4$ km, or roughly seven white dwarf radii. The gas subsequently accretes along the field lines in the manner of an auroral curtain or arc. A strong shock is produced just above the surface, with the hot gas ($kT \sim 20$ keV) cooling via bremsstrahlung emission, producing a luminosity of 5–10 $\times\ 10^{34}$ ergs s^{-1}. Electron scattering within the accretion curtain produces the effect of nonisotropic emission of the harder X-rays (2–10 keV), resulting in a fan-beam perpendicular to the curtain. As the white dwarf spins, this beam sweeps over the system, and a high fraction (>50%) of the incident X-rays are reprocessed in the accretion disk, its hot spot, and the inner face of the secondary star into optical radiation. The soft X-ray (0.1–2 keV) modulation at the white dwarf spin period is explained in terms of varying line-of-sight photoionization opacity, while the harder X-rays (2–10 keV) are modulated predominantly at the sideband period $\nu - \omega$ (2106 s), due to reflection off the secondary and hot spot, where the dominant optical periodicity arises. The model is capable of explaining the following properties: (1) the flux distribution; (2) the optical and X-ray periods and their pulse fractions; (3) the emission-line shape, structure, and velocity variations. A schematic representation of the model is shown in Figure 20.

We conclude that the spin-modulated velocities cannot be explained by the illumination of a region of the disk (i.e., the searchlight model). Our explanation of the velocities being produced at the disk/magnetosphere interface are supported by observations of other systems.

Furthermore, we show that the magnetospheric gating model, with the requirement that no accretion disk is present, is inapplicable for 1H0542−407 unless the magnetic field strength is inordinately high (>40 MG). Our model predicts a field strength in the region 1–10 MG.

We note that recent observations of 1H0542−407 (1988 March) have shown the system to be ~ 1 mag brighter than during 1985, and we consequently urge continued monitoring of this most interesting system. Also, careful photometric studies in the future may yield values for $\dot{P}_{\rm spin}$ and, in turn, constrain the mass transfer parameter and give a more accurate magnetic field value.

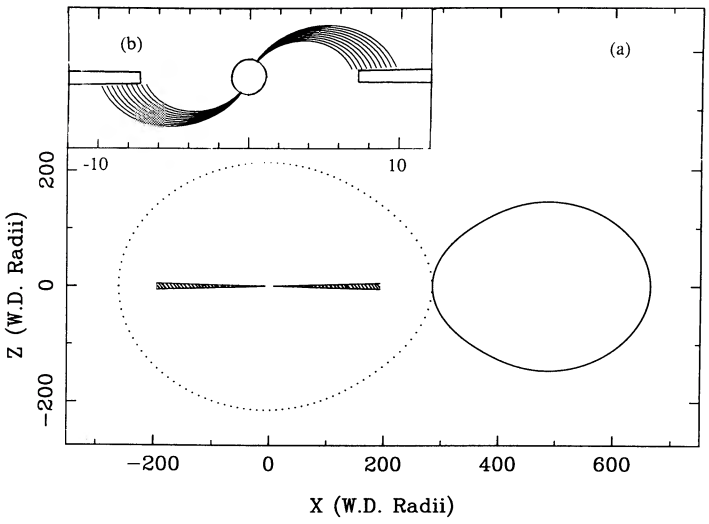

FIG. 20*a*, *b*

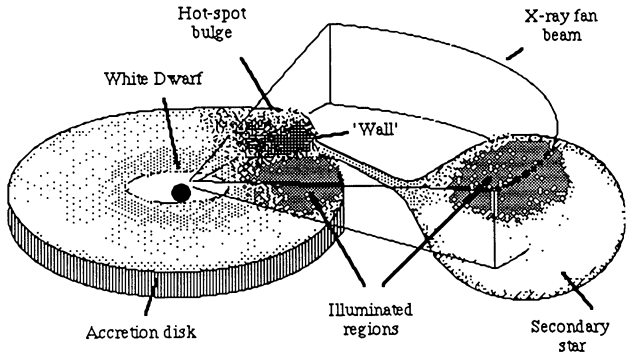

FIG. 20*c*

FIG. 20.—(*a*) The Roche geometry and schematic diagram of our model (to scale) for 1H0542−407. (*b*) Expansion of the inner disk, with the magnetic field lines intersecting the disruption region on the disk. (*c*) Schematic representation of the model derived for 1H0542−407.

We are grateful to Dayal Wickramasinghe for useful discussions and comments. Thanks are due to Jeremy Bailey and the staff of the AAT for help given during our high-speed IPCS run. We also wish to thank the Director of the Anglo-Australian Observatory, R. Cannon, for the allocation of infrared service time. We also wish to acknowledge the help of the ANU staff at SSO for their support during our 2.3 m runs.

Finally, we point our that this work follows from a most successful collaboration with our colleagues Ron Remillard, Hale Bradt (MIT), and Dan Schwartz (CfA), involving the optical identification of the weak X-ray sources detected by the *HEAO 1* Modulation Collimator (A-3) experiment, under the US/Australia Cooperative Science Program.

D. A. H. B. acknowledges support of an ANU postgraduate scholarship.

REFERENCES

Allen, C. W. 1973, *Astrophysical Quantities* (3d ed.; London: Athlone).
Anzer, U., and Börner, G. 1980, *Astr. Ap.*, **83**, 133.
———. 1983, *Astr. Ap.*, **122**, 73.
Bailey, J. 1981, *M.N.R.A.S.*, **197**, 31.
———. 1984, Anglo-Australian Observatory User Manual No. 13.
Basko, M. M., and Sunyaev, R. A. 1973, *Ap. Space Sci.*, **23**, 117.

Basko, M. M., Sunyaev, R. A., and Titarchuk, L. G. 1974, *Astr. Ap.*, **31**, 249.
Bath, G. T., Evans, W. D., Papaloizou, J., and Pringle, J. E. 1974, *M.N.R.A.S.*, **169**, 447.
Berriman, G. 1988, in *Proc. Vatican Conf. on Circumstellar Polarization* (Rome: Specola Vaticana), in press.
Bessell, M. S. 1979, *Pub. A.S.P.*, **91**, 589.
Bessell, M. S., and Brett, J. M. 1988, *Pub. A.S.P.*, in press.
Buckley, D. A. H., and Tuohy, I. R. 1987, *Proc. Astr. Soc. Australia*, **7**, 151.
Buckley, D. A. H., Tuohy, I. R., and Remillard, R. A. 1985, *Proc. Astr. Soc. Australia*, **6**, 147.
Chanan, G. A., Nelson, J. E., and Margon, B. 1978, *Ap. J.*, **226**, 963.
Chanmugam, G., and Frank, J. 1987, *Ap. J.*, **320**, 746.
Chanmugam, G., and Ray, A. 1984, *Ap. J.*, **285**, 252.
Córdova, F. A., and Mason, K. O. 1983, in *Accretion Driven Stellar X-Ray Sources*, ed. W. H. G. Lewin and E. P. J. van den Heuvel (Cambridge: Cambridge University Press), p. 147.
Cropper, M. 1986, *M.N.R.A.S.*, **222**, 225.
Deeming, T. J. 1975, *Ap. Space Sci.*, **4**, 193.
Eggleton, P. P. 1983, *Ap. J.*, **268**, 368.
Faulkner, J. 1971, *Ap. J.* (*Letters*), **170**, L99.
Felsteiner, J., and Opher, R. 1976, *Astr. Ap.*, **46**, 189.
Frank, J., King, A. R., and Raine, D. J. 1985, *Accretion Power in Astrophysics* (Cambridge: Cambridge University Press), p. 86.
Hassall, B. J. M., *et al.* 1981, *M.N.R.A.S.*, **197**, 275.
Hameury, J.-M., King, A. R., and Lasota, J.-P. 1986, *M.N.R.A.S.*, **218**, 695.
Hameury, J.-M., King, A. R., Lasota, J.-P., and Ritter, H. 1987, *Ap. J.*, **316**, 275.
Hellier, C., Mason, K. O., Rosen, S. R., and Córdova, F. A. 1987, *M.N.R.A.S.*, **228**, 463.
Hessman, F. V. 1988, *Astr. Ap. Suppl.*, **72**, 515.
Honeycutt, R. K., Schlegel, E. M., and Kaitchuck, R. H. 1986, *Ap. J.*, **302**, 388.
Horne, K., and Marsh, T. R. 1986, *M.N.R.A.S.*, **218**, 761.
Hutchings, J. B., and Coté, T. J. 1986, *Pub.A.S.P.*, **98**, 104.
Imamura, J. N., and Durisen, R. H. 1983, *Ap. J.*, **268**, 291.
Kaitchuck, R. H., Hantzios, P. A., Kakaletris, P., Honeycutt, R. K., and Schlegel, E. M. 1987, *Ap. J.*, **317**, 765.
King, A. R. 1985, in *Proc. ESA Workshop, Recent Results on Cataclysmic Variables*, ed. W. R. Burke (ESA SP-236), p. 133.
King, A. R., Frank, J., and Ritter, H. 1985, *M.N.R.A.S.*, **213**, 181.
King, A. R., and Shaviv, G. 1984, *M.N.R.A.S.*, **211**, 883.
Lamb, D. Q. 1983, in *Cataclysmic Variables and Related Objects*, ed. M. Livio and G. Shaviv (Dordrecht: Reidel), p. 299.
———. 1985, in *Cataclysmic Variables and Low-Mass X-Ray Binaries*, ed. D. Q. Lamb and J. Patterson (Dordrecht: Reidel), p. 179.
Lamb, D. Q., and Mason K. O. 1986, in preparation.
Lamb, D. Q., and Melia, F. 1987, *Ap. Space Sci.*, **131**, 511.
Lamb, D. Q., and Patterson, J. 1983, in *Cataclysmic Variables and Related Objects*, ed. M. Livio and G. Shaviv (Dordrecht: Reidel), p. 229.
Liebert, J., and Stockman, H. S. 1985, in *Cataclysmic Variables and Low-Mass X-Ray Binaries*, ed. D. Q. Lamb and J. Patterson (Dordrecht: Reidel), p. 151.
Lynden-Bell, D. 1969, *Nature*, **233**, 690.
Mason, K. O. 1985, private communication.
Mason, K. O. 1985, *Space Sci. Rev.*, **40**, 99.
Mason, K. O., Rosen, S. R., and Hellier, C. 1987, in *The Physics of Compact Objects* (New York: Pergamon).
McHardy, I. M. Pye, J. P., Fairall, A. P., and Menzies, J. W. 1987, *M.N.R.A.S.*, **225**, 355.
Milgrom, M., and Salpeter, E. E. 1975*a*, *Ap. J.*, **196**, 583.
———. 1975*b*, *Ap. J.*, **196**, 589.
Mouchet, M., Bonnet-Bidaut, J. M., Ilovaisky, S. A., and Chevalier, C. 1981, *Astr. Ap.*, **102**, 31.
Nauenberg, M. 1972, *Ap. J.*, **175**, 417.
Patterson, J. 1984, *Ap. J. Suppl.*, **54**, 443.
Patterson, J., and Price, C. M. 1981, *Ap. J.* (*Letters*), **243**, L83.
Patterson, J., and Steiner, J. E. 1983, *Ap. J.* (*Letters*), **264**, L61.
Penning, W. R. 1985, *Ap. J.*, **289**, 300.
Penning, W. R., Schmidt, G. D., and Liebert, J. 1986, *Ap. J.*, **301**, 885.
Rappaport, J., Verbunt, F., and Joss, P. C. 1983, *Ap. J.*, **275**, 713.
Robinson, E. L. 1987, *Ap. Space Sci.*, **130**, 113.
Rosen, S. R., Mason, K. O., and Córdova, F. A. 1988, *M.N.R.A.S.*, **231**, 549.
Schmidt, G. D., and Liebert, J. 1987, *Ap. Space Sci.*, **131**, 549.
Schneider, D. P., and Young, P. 1980, *Ap. J.*, **238**, 946.
Schwarz, H. E., and Heemskerk, M. H. M. 1987, *IAU Circ.*, No. 4508.
Shafter, A. W. 1983, Ph.D. thesis, UCLA.
———. 1985, in *Cataclysmic Variables and Low-Mass X-Ray Binaries*, ed. D. Q. Lamb and J. Patterson (Dordrecht: Reidel), p. 355.
Shafter, A. W., Szkody, P., and Thorstensen, J. R. 1986, *Ap. J.*, **308**, 765.
Shafter, A. W., and Targon, D. M. 1982, *A.J.*, **87**, 655.
Shafter, A. W., Wheeler, J. C., and Cannizzo, J. K. 1986, *Ap. J.*, **305**, 261.
Shakura, N. I., and Sunyaev, R. A. 1973, *Astr. Ap.*, **24**, 337.
Sulkanen, M. E., Brasure, L. W., and Patterson, J. 1981, *Ap. J.*, **244**, 579.
Swank, J. H., Fabian, A. C., and Ross, R. R. 1984, *Ap. J.*, **280**, 734.
Tuohy, I. R., Buckley, D. A. H., Remillard, R. A., Bradt, H. V., and Schwartz, D. A. 1986, *Ap. J.*, **311**, 275 (Paper I).
Verbunt, F., and Zwaan, C. 1981, *Astr. Ap.*, **100**, L7.
Wade, R. A. 1985, in *Interacting Binaries*, ed. P. P. Eggleton and J. E. Pringle (Dordrecht: Reidel), p. 289.
Warner, B. 1973, *M.N.R.A.S.*, **162**, 189.
———. 1974, *M.N.R.A.S.*, **168**, 235.
———. 1983, *IAU Colloquium 72, Cataclysmic Variables and Related Objects*, ed. M. Livio and G. Shaviv (Dordrecht: Reidel), p. 155.
———. 1985, in *Cataclysmic Variables and Low-Mass X-Ray Binaries*, ed. D. Q. Lamb and J. Patterson (Dordrecht: Reidel), p. 269.
———. 1986, *M.N.R.A.S.*, **219**, 347.
Warner, B., and Cropper, M. 1984, *M.N.R.A.S.*, **206**, 261.
Watts, D. J., Bailey, J., Hill, P. W., Greenhill, J. G., McCowage, C., and Carty, T. 1986, *Astr. Ap.*, **154**, 197.
West, S. C., Berriman, G., and Schmidt, G. D. 1987, *Ap. J.* (*Letters*), **322**, L35.
White, N. E., and Marshall, F. W. 1981, *Ap. J.* (*Letters*), **249**, L25.
Wickramasinghe, D. T. 1988, in *Proc. Vatican Conf. on Circumstellar Polarization* (Rome: Specola Vaticana), in press.
Wickramasinghe, D. T., Stobie, R. S., and Bessell, M. S. 1982, *M.N.R.A.S.*, **200**, 605.

D. A. H. BUCKLEY: Department of Astronomy, University of Cape Town, Rondebosch 7700, Cape Town, South Africa

I. R. TUOHY: British Aerospace Australia, P.O. Box 180, Salisbury, South Australia 5108, Australia